

SPECTRAL ATLAS OF X-RAY LINES EMITTED DURING SOLAR FLARES BASED ON CHIANTI

E. LANDI

Artep, Inc., Ellicott City, MD 21042; and Naval Research Laboratory, Washington, DC 20375-5320

AND

K. J. H. PHILLIPS

National Research Council Senior Research Associate, NASA Goddard Space Flight Center, Greenbelt, MD 20771

Received 2005 February 14; accepted 2005 May 16

ABSTRACT

A spectral atlas of X-ray lines in the wavelength range 7.47–18.97 Å is presented, based on high-resolution spectra obtained during two M-class solar flares (on 1980 August 25 and 1985 July 2) with the Flat Crystal Spectrometer on board the *Solar Maximum Mission*. The physical properties of the flaring plasmas are derived as a function of time using strong, unblended lines. From these properties, predicted spectra using the CHIANTI database have been obtained, which were then compared with wavelengths and fluxes of lines in the observed spectra to establish line identifications. Identifications for nearly all the observed lines in the resulting atlas are given, with some significant corrections to previous analyses of these flare spectra. Line ratios allowed us to determine temperature and density; in the 1985 July 2 flare, very high densities ($N_e \simeq 10^{13} \text{ cm}^{-3}$) were measured.

Subject headings: line: identification — plasmas — Sun: flares — Sun: X-rays, gamma rays

1. INTRODUCTION

The X-ray wavelength range between 5 and 20 Å has been a prime resource for the investigation of high-energy phenomena in the solar atmosphere, owing to the presence of a large number of spectral lines from highly ionized stages of the most abundant elements. The analysis of the fluxes of these lines, and of the continuum radiation also observed in this wavelength range, has allowed the measurement of the main physical parameters in solar active regions and flares since the beginning of space science.

Several spectral atlases encompassing this wavelength range have been developed to help in the identification of the observed spectral features. In most cases, such spectral atlases were developed basing line identifications on wavelengths, trying to match the observed values with those predicted by atomic codes. In some cases, oscillator strengths as an indicator of line intensities were also used to assist identifications. Only a few line lists have been compiled in which observed line fluxes are compared with fluxes calculated using transition rates and other atomic data. Line fluxes are of great help in the identification of spectral features, but they require a large amount of atomic data. Unfortunately, until the recent past, the atomic physics data available for such purposes were of limited quantity.

Several efforts have been made to improve the knowledge of the atomic physics underlying the X-ray emission in order to develop diagnostic tools that could allow both accurate X-ray line identifications and plasma diagnostic studies. This effort led to the first spectral codes ever developed (Landini & Monsignori Fossi 1970; Mewe 1972). These spectral codes have been continually updated over the years, and new ones have appeared since, in particular CHIANTI (Dere et al. 1997; Young et al. 2003) and APEC/APED (Smith et al. 2001). These spectral codes have been widely used for the analysis of both high-resolution and narrowband images obtained by instruments on various space missions. One crucial issue in the development of such spectral codes is their completeness, since several portions of the X-ray range are crowded with spectral

lines, and blending is a significant issue when observed spectra are used for plasma diagnostics. In recent years, improvements in computer technology have made it possible to calculate vast amounts of atomic data in the X-ray range, providing a unique opportunity for the development of accurate and comprehensive X-ray spectral atlases.

Recently, some new extensive atomic physics calculations have been carried out in an effort to provide the necessary data for calculating line emission from high-energy configurations in the ions Fe XVII–XXIII (Landi & Gu 2005). These calculations include all the relevant processes contributing to level populations for those ions, whose lines dominate most of the 7–19 Å range of solar flare spectra. Coupled with the CHIANTI database, this data set provides a formidable tool for evaluating line emissivities for all possible transitions and ions in this range, thus enabling the development of a comprehensive and accurate spectral atlas taking full account of line blending. The aim of the present paper is to apply this combined data set to develop a complete atlas of solar flare X-ray spectra in the 7–19 Å range.

The observations used to achieve our goal were taken with the Flat Crystal Spectrometer (FCS) on board the *Solar Maximum Mission* (SMM) during flares on 1980 August 25 and 1985 July 2. Data from the companion Bent Crystal Spectrometer (BCS) were available throughout the FCS wavelength scans of each flare. For the August 25 flare, an extensive analysis of the FCS data taken during the flare decay (Phillips et al. 1982) resulted in a list of 205 lines in the 5.68–18.97 Å range with identifications provided. A benchmark analysis was done using these same data with the MEKAL code (Mewe et al. 1995) by Phillips et al. (1999), with adjustments to the wavelengths and additions of some lines to the MEKAL database to match the observations. Neither of these analyses used BCS data, which contain important information about the flaring plasma. It is possible to analyze the BCS and FCS data grouped in short time intervals during the wavelength scans, something not done by Phillips et al. (1982), while the FCS data were similarly grouped in five short sections of the total scan in the work of Phillips et al.

(1999). At the time of the 1985 July 2 flare, only four of the seven FCS channels were operating. Unlike the 1980 August 25 flare, the peak of the flare (which was marginally more intense) was observed. Thus, higher ionization stages were present in the spectra. This data set is used to complement the 1980 August 25 one.

The August 25 flare spectra have been completely reanalyzed: FCS and BCS line fluxes have been remeasured with calibration factors applied, and BCS spectra analyzed to give temperature and emission measure as a function of time. The observations have been divided into seven time bins, with mean values of temperature and emission measure derived for each, and synthetic spectra calculated using the CHIANTI database and code. The resulting predicted line list has been compared with the observed spectra to establish line identifications. A more detailed comparison involving observed and calculated line fluxes for individual lines and ions is beyond the scope of the present work and is deferred to a future paper (Landi et al. 2005b).

In § 2 we describe the instruments, and the observations are outlined in § 3. Section 4 reviews the diagnostic methods used to measure the physical parameters of the emitting plasma, and results for the August 25 flare spectrum are given in § 5. Results for the July 2 spectrum are reported in § 6. The final line lists are given in § 7, and results are summarized in § 8.

2. THE INSTRUMENTS

For nearly 10 years, from its launch on 1980 February 14 to the re-entry in the Earth's atmosphere on 1989 December 2, the NASA solar flare mission *Solar Maximum Mission* recorded many thousands flares with its complement of seven instruments. One of these, the X-ray Polychromator (Acton et al. 1980), viewed flare and active region emission in the soft X-ray range. Its two parts, the Bent Crystal Spectrometer (BCS) and Flat Crystal Spectrometer (FCS), were spectrometers with spectral resolution that was at the time, and for some spectral regions remains still, unprecedentedly high.

The BCS consisted of eight curved crystals with solar X-rays incident via a coarse grid collimator ($6'$ FWHM) and position-sensitive proportional counters, one for each crystal. The wavelength range, 1.769–1.947 and 3.165–3.231 Å, covered lines of highly ionized Fe atoms, including H-like (Fe xxvi) and He-like (Fe xxv) Fe ions, the $K\alpha$ fluorescence lines of photospheric Fe, visible during intense disk flares, and lines due to He-like Ca (Ca xix) ions. Dielectronic satellite lines visible in BCS spectra near the He-like and H-like ion lines are of diagnostic importance, enabling electron temperatures T_e to be measured. Spectra over the complete range of each of the eight channels were formed simultaneously in data gathering intervals as short as 9 s. Flare continuum radiation is detected in the Ca xix channel, though not in the other seven channels for which a crystal fluorescence background masks the continuum.

The FCS had seven channels with nominal wavelength coverage 1.40–22.43 Å. Their wavelength ranges are listed in Table 1. The flat crystals were mounted on a single rotatable shaft, with a proportional counter viewing the spectra produced by each crystal. High-precision closed-loop servo drive-encoder units at either end of the shaft, operating independently, drove the crystal shaft at preprogrammed rates (in steps of $9''/89$ arc) and ranges. At a particular orientation, the “home” position, prominent spectral lines were simultaneously observed by the seven proportional counters. These included the resonance lines (transition $1s^2\ ^1S_0 - 1s2p\ ^1P_1$ lines also known as w) of He-like He, Mg,

TABLE 1
WAVELENGTH RANGES FOR THE FLAT CRYSTAL SPECTROMETER ON BOARD *SMM*

Channel Number	H.P. (Å)	λ_{\min} (Å)	λ_{\max} (Å)	H.P. Line
1.....	18.97	13.10	22.43	O VIII Ly α
2.....	13.45	10.56	14.94	Ne IX w
3.....	9.17	7.33	10.09	Mg XI w
4.....	6.65	4.93	7.61	Si XIII w
5.....	5.04	3.63	5.84	S XV w
6.....	3.17	2.38	3.61	Ca XIX w
7.....	1.85	1.40	2.10	Fe XXV w

NOTES.—The “H.P. line” is the strong line at the home position (H.P.) in each channel. The transition of w is $1s^2\ ^1S_0 - 1s2p\ ^1P_1$.

Si, S, Ca, and Fe (channels 2–7, respectively); the home position of channel 1 was marked by the Ly α line of H-like O. The determination of line wavelengths depends only on the chosen wavelength of the home position lines, since the relative scale is extremely precise. Phillips et al. (1982) estimated that the wavelength precision for channels 1, 3, and 4 was 0.001 Å, and better than 0.001 Å for channel 2.

Solar X-rays were incident on the flat crystals via a 1 m long, fine-wire collimator with FWHM $14''$. The spectrometer had two modes of operation. In an imaging mode, the spectrometer could form images, typically a few arcminutes on a side, of active region or flare emission by a boustrophedonic scanning motion, with drives in x and y directions over the image, with the crystal shaft locked in its home position. In a spectral mode, the FCS was pointed at a fixed location on the Sun and the crystal shaft driven over preprogrammed spectral ranges. Independent microprocessors controlled the operation of both BCS and FCS. Increasing X-ray emission during a flare, detected by the BCS, would initiate a flare “flag,” which would interrupt FCS spatial scans of an active region and trip the FCS into a preprogrammed spectral scan or some other spatial scan.

During normal operations, *SMM* was finely pointed at the Sun center, allowing individual instruments like the FCS to offset-point to particular solar active regions showing promise of flare productivity. Full operations of all *SMM* instruments were possible from launch till 1980 November, when the third of four attitude control units failed, after which only coarse Sun-pointing was possible and only the full-Sun field of view instruments on *SMM* could continue to operate. The Space Shuttle *SMM* Repair Mission (STS 41-C) in 1984 April, in which *SMM* was successfully docked with the Space Shuttle and its faulty attitude control unit replaced, enabled normal operations to continue for five more years. The FCS had performed only a few spectral scans in the first (1980) mission, an early failure of one of the two crystal drive units necessitating some caution in the use of the remaining unit. However, solar activity had declined sharply from its maximum in late 1979, so that there was increased urgency in the use of the spectral scanning capabilities of the FCS after the Shuttle repair mission. By this time, some of the detectors had failed, so crystal scans were incomplete after 1984. Through this turn of events, only a single full crystal scan was accomplished in the lifetime of *SMM*, obtained during the 1980 August 25, under discussion here.

Data from both the BCS and FCS are stored at NASA Goddard Space Flight Center and various other locations around the world and can be accessed and analyzed by IDL software in the

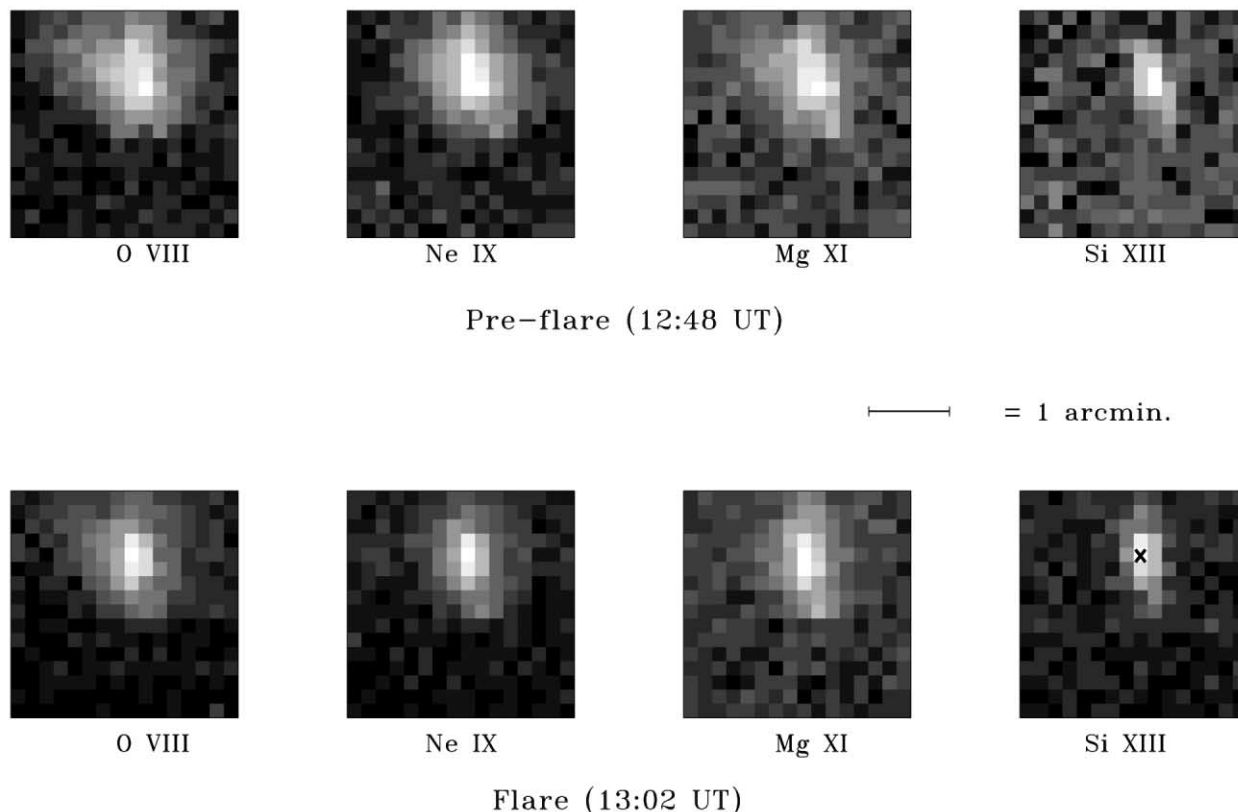


FIG. 1.—FCS flux maps of the 1980 August 25 flaring region, before the flare (*top row*) and shortly after the flare onset (*bottom row*). The ions shown under each image indicate the lines, which are the H-like Ly α of O VIII (formed at $\approx 3 \times 10^6$ K) and the He-like resonance w lines of Ne IX ($\approx 4.5 \times 10^6$ K), Mg XI ($\approx 6.3 \times 10^6$ K), and Si XIII ($\approx 8.9 \times 10^6$ K). The cross in the bottom right Si XIII panel indicates the location at which the full FCS spectral scan was taken.

Solarsoft package. Calibration factors and other instrumental parameters are also available at these sites.

3. THE OBSERVATIONS

The 1980 August 25 flare was of *GOES* class M1.5, with optical importance SB (subflare, bright), from disk active region NOAA 2629 (N20°, W26°). *SMM* had emerged from spacecraft night at 12:45 UT, shortly before the flare occurred. Flare maximum brightness occurred at 13:09 UT. The FCS performed two $4' \times 4'$ rasters, immediately before the flare onset and then after the flare started. Intensity maps from these rasters in O VIII, Ne IX, Mg XI, and Si XIII are displayed in Figure 1. The FCS was then repositioned to the location of maximum emission in channel 5, viewing the He-like S (S XV) line at home position. Eight short spectral scans of the home position were then performed between 13:07 and 13:10 UT. Data from the BCS, operating in a routine mode, show that the Ca XIX emission had reached its maximum at 13:06 UT. The FCS crystal shaft was then driven to its short-wavelength limit and a continuous scan, in $50''$ steps and dwell time 0.512 s at each location, was performed. The scan lasted for 17 minutes, starting after the flare peak, so that only the decay phase of the event was recorded in the complete spectral scan. The total emission in the BCS Ca XIX channel had declined from 16,000 to 5690 photons $\text{cm}^{-2} \text{s}^{-1}$ in the time of the scan that finished at 13:28 UT. Figure 2 shows the total flux of the BCS Ca XIX channel from before the flare onset to late into the decay phase.

The 1985 July 2 event was of *GOES* class M4.5, starting at 21:00 UT, peaking at 21:27 UT, with decay lasting till at least 23:20 UT, at the end of the following *SMM* orbit. At the time

of this flare, three of the seven detectors were either switched off or not working, thus leaving gaps in the wavelength coverage. Smaller gaps occurred in the data because of breaks in transmission from the tracking station, that corrupted a few lines such as the Mg XI $1s3p$ and Mg XI $1s2p$ resonance lines, and data from channel 1 (13.10–18.97 Å), although transmitted to the ground, are not available. The FCS spectral scan started at

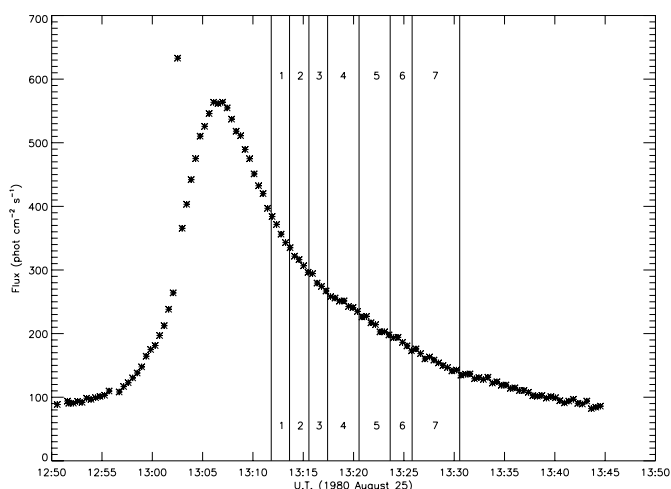


FIG. 2.—Total flux in the BCS Ca XIX channel during the 1980 August 25 flare as a function of time. The time bins corresponding to the FCS analysis (see § 2) are also shown. The high flux at 13:03 UT is not real but is due to cross-talk from the FCS microprocessor occurring when the FCS crystal drive was turned on.

around 21:10 UT and lasted some 27 minutes, thus encompassing the rise, peak and decay phase of the flare. For the present work, we will focus only on the data from channel 3 (7.33–10.09 Å) and the BCS Ca XIX window at around 3.20 Å, since the other working FCS channels either were unavailable or the data from them were too noisy to be analyzed.

4. PLASMA DIAGNOSTICS TECHNIQUES

An accurate line list requires identifications based on both predicted and observed wavelengths and fluxes. Line fluxes can only be predicted once the physical parameters of the emitting plasma are known. In order to measure the plasma physical parameters and to predict accurate line emission it is necessary to use a complete and up-to-date plasma emission code.

In the present work, we will use the CHIANTI database both as a source of wavelengths and line fluxes, and as a tool to determine the physical properties of the emitting plasma. The CHIANTI database is particularly well suited for this study, since it has been recently expanded to include a vast number of configurations and fine-structure levels (from Landi & Gu 2005) that allow the calculation of all significant X-ray lines (as well as other data), constituting version 5 of the database (Landi et al. 2005a).

Recent studies of flare plasma carried out using *SOHO* SUMER observations in the ultraviolet wavelength range suggested that the thermal structure of the flaring plasma is nearly isothermal and very slowly varying with time (Landi et al. 2003). The rate of temperature decrease measured by Landi et al. (2003) was sufficiently low that, if applied to the present observation, it implies that the plasma has nearly constant temperature during the whole observation. If these results also apply to the present data sets, the measurement of plasma thermal properties and the calculation of a synthetic spectrum becomes relatively straightforward.

In order to verify whether the SUMER results also apply to the present flare, we will measure the plasma temperature using different methods, as described below. Consistency of the results will provide an indication that the plasma is indeed isothermal. In both cases, emissivities from the CHIANTI database have been calculated adopting coronal abundances (Feldman et al. 1992) and using the ion fractions from Mazzotta et al. (1998), under the assumption of ionization equilibrium. This is justified by the probable value of ionization times, only a few seconds for probable values of the flare density ($\geq 10^{11} \text{ cm}^{-3}$), which are much smaller than the timescales for the observed temperature changes.

4.1. Emission Measure Analysis

Pottasch (1963) first introduced an emission measure analysis based on ultraviolet lines, the principle of which we follow here. The flux of an optically thin line emitted by an isothermal plasma at distance d ($=1 \text{ A.U.}$) can be written as

$$F_i = \frac{1}{4\pi d^2} G_i(T_e, N_e) \langle \text{EM} \rangle, \quad \langle \text{EM} \rangle = \int_V N_e^2 dV, \quad (1)$$

where N_e and T_e are the plasma electron density and temperature, V is the emitting volume, $G_i(T_e, N_e)$ is the contribution function of the emitting line, which for most X-ray lines depends strongly on electron temperature but only weakly if at all on density, and $\langle \text{EM} \rangle$ is the volume emission measure of the

plasma. The diagnostic method consists of calculating the function $\langle \text{EM}(T) \rangle$ defined as

$$\langle \text{EM}(T) \rangle = 4\pi d^2 \frac{F_i}{G_i(T_e, N_e)} \quad (2)$$

as a function of electron temperature T_e , using the observed fluxes F_i of each observed line i and the electron density derived from the line ratio techniques. When all the $\langle \text{EM}(T) \rangle$ curves are displayed in the same plot as a function of temperature, these curves should intersect at a common point $(T_e, \langle \text{EM}(T) \rangle)$, if the plasma is isothermal. Given the observational uncertainties, the $\langle \text{EM}(T) \rangle$ curves will define a narrow range in the T_e - $\langle \text{EM} \rangle$ space where they all cross. The crossing point and its uncertainties are determined as the region where the largest number of the $\langle \text{EM}(T) \rangle$ curves meet, and the plasma temperature and emission measure with their uncertainties can be derived. Examples are given in Figure 4.

4.2. Analysis of the BCS Ca XIX Channel Data

A second method was used to determine temperature and EM during the flare using the Ca XIX emission observed by the BCS. Temperature T_e is determined from the flux ratio of the Ca XIX 3.177 Å w line and the Ca XVIII dielectronic satellite line k , where, according to the notation first used by Gabriel (1972), w corresponds to the Ca XIX transition $1s^2 \ ^1S_0 - 1s2p \ ^1P_1$ and k corresponds to the Ca XVIII dielectronic transition $1s^2 2p^2 \ ^2P_{1/2} - 1s2p^2 \ ^2D_{3/2}$. From this value of T_e , the emission measure can be determined from the flux of the Ca XIX w line or of the continuum emission, and CHIANTI-derived emissivities. Comparison between the line-based and the continuum-based emission measure values provide a check on the robustness of the results.

In order to take into account the time variability of the flare plasma, we have divided the BCS observation corresponding to the FCS spectral scan in several time bins of similar duration. Gaussian line profiles were fitted to spectral line features, and the continuum background was evaluated in each time bin. The line profiles in principle depart from a Gaussian (being a convolution of the crystal rocking curve and the thermal Doppler profile), but a Gaussian profile was found to be an adequate representation for all lines.

4.3. Diagnostics Using Line Ratios among Fe Ions

Ratios between lines of the same ions emitted by levels in configurations with very different excitation energy are usually excellent indicators of the electron temperature. Unfortunately, in the present data set such ratios usually involve lines observed in different channels, and their relative flux calibration is too uncertain to provide reliable results. However, in a few cases there are pairs of Fe lines with similar wavelengths and different upper configuration, so they can be used for temperature diagnostics.

A few density-sensitive line ratios involving lines emitted by the same Fe ion are available in the X-ray range, but most of them are sensitive to densities in excess of 10^{12} cm^{-3} , greater than likely values in the August 25 flare, but possibly useful for measuring the electron density in the July 2 flare. Some of the density sensitive lines (i.e., Fe XX 12.888 Å, Fe XXI 12.327 Å) are too weak to be detected at densities $\leq 10^{11} \text{ cm}^{-3}$, so in case they are not observed, an upper limit to the electron density can be given.

4.4. Diagnostics Using He-like Line Ratios

The He-like lines emitted by the $1s2l$ configurations can be used both for density and temperature diagnostics. In particular, the ratio $R = I(1s^2\ ^1S_0-1s2p\ ^3P_{1,2})/I(1s^2\ ^1S_0-1s2s\ ^3S_1) = (x+y)/z$ is weakly dependent on the electron temperature but is strongly dependent on the electron density, so that this latter quantity can be measured. However, it is necessary to consider the presence of blending satellite lines to both lines. The ratio $G = [I(1s^2\ ^1S_0-1s2p\ ^3P_{1,2}) + I(1s^2\ ^1S_0-1s2p\ ^3S_1)]/I(1s^2\ ^1S_0-1s2p\ ^1P_1) = (x+y+z)/w$ is dependent on temperature, but not on density, so that it can be used as a temperature indicator.

These ratios can be measured in the August 25 data set for Ne ix, Mg xi, and Al xii. Also Na x is present, but its $1s^2\ ^1S_0-1s2p\ ^1P_1$ line is blended with a stronger Ne ix line and cannot be used for temperature diagnostics.

4.5. Diagnostics Using H-like Line Ratios

The August 25 data set also includes a few H-like lines, from O viii, Ne x, and Mg xii. A few components of the Lyman series were observed for O viii, Ne x, and Mg xii: $Ly\alpha$, $Ly\beta$, and $Ly\gamma$ for O viii, $Ly\alpha$, $Ly\beta$ for Ne ix, and $Ly\alpha$ for Mg xi. Ratios between lines in the Lyman series are excellent temperature indicators, but they are sensitive to temperatures below those expected for the flares analyzed here. Also, they might be affected by optically depth effects.

4.6. Diagnostics Using Dielectronic Satellite Lines

The intensity ratio of a Li-like ion dielectronic satellite line (formed purely by dielectronic recombination) to line w of the He-like ion is sensitive to electron temperature T_e (approximately T_e^{-1}) but not ion fractions; see Gabriel (1972) for details. This fact was used here to measure temperatures from the Ca xviii dielectronic line k to the Ca xix w line ratio, observed by the BCS in both flares analyzed here. Several other satellites can be identified in the flare spectra discussed here, including corresponding satellites in He-like Mg and Al spectra and $n = 3$ satellites. A prominent satellite feature (sometimes called J) due to He-like ions occurs near the H-like $Ly\alpha$ lines of some ions and is similarly useful for temperature determination.

5. RESULTS: 1980 AUGUST 25 FLARE

Since the flaring plasma cools significantly with time, we have divided the August 25 data set into seven time bins, whose duration has been chosen as a compromise between the need of including in each time bin enough lines of different ions to provide a reliable EM measurement in at least one channel, and the need to limit the changes in the plasma physical parameters in each time bin. This latter requirement was met by limiting the change in total flux in the BCS Ca xix flux to 25%. Table 2 gives the time bin list, and the ions included in each time bin. Their relation to the onset of the flare and to the total BCS Ca xix flux is displayed in Figure 2. Figure 3 shows the wavelength ranges included in each time bin. A set of unblended lines for the emission measure (EM) analysis was selected through a preliminary comparison of the observed spectra and a CHIANTI synthetic spectrum calculated using the average flare differential emission measure available in the CHIANTI database (based on the data from Dere & Cook 1979).

5.1. Emission Measure Analysis

The emission measure analysis outlined in § 4.1 was applied to each time bin listed in Table 2, and results are given in

TABLE 2

TIME BIN SELECTED FOR THE ANALYSIS OF THE 1980 AUGUST 2 FCS SPECTRUM

Time Bin	Δt (s)	Time (UT)	Ions
1.....	0–100	13:10:00–13:11:40	Fe xvii, xviii, xix, xx, xxiii, Ni xix
2.....	100–206	13:11:40–13:13:26	Fe xvii, xviii, xix, xx
3.....	206–308	13:13:26–13:15:14	Fe xvii, xviii, xix, xxii, xxiii, Ni xx
4.....	308–486	13:15:14–13:18:06	Fe xvii, xx, xxi
5.....	486–656	13:18:06–13:20:56	Fe xviii, xix, xx
6.....	656–776	13:20:56–13:22:56	Fe xvii, xix, Ni xix
7.....	776–1036	13:22:56–13:27:36	Fe xviii, xix

NOTES.—The value of Δt is the time measured from 13:10:00 UT. “Ions” indicates ions whose emission lines are present in the time bin.

Figure 4. Results for time bin 3 (channel 2) and time bin 7 are not displayed since there were not enough ions to provide any reliable crossing point. Because of the paucity of lines, the EM analysis could not be applied to any channel 3 lines. No channel 1 lines are available for time bins 4–7. For the same time bin, more than one EM plot may be shown. In fact, lines of different channels were available for nearly all time bins, but since there is some uncertainty in the relative flux calibration of FCS channels, we applied the EM analysis to lines from the same FCS channel. In all the other channels, lines from 3 to 5 different ions were available for the analysis, with the only exception of channel 2, time bin 2, for which only two ions could be used: results for this data set are more uncertain but they are also shown as a check on the results of channel 1, time bin 1.

Figure 4 shows that for all the cases considered, a crossing point could be identified. The ions included in each plot in Figure 4 range from Fe xvii to Fe xxiii. The EM values measured in the same time bin with channel 1 and 2 lines are similar, indicating that the relative flux calibration of these two channels is correct within the uncertainties (less than 0.2 in the log). The existence of a crossing point defined by such a wide span of ion stages of Fe indicates that the flare plasma that generates the Fe emission is indeed close to isothermal within each time bin.

Figure 4 also shows that the EM curves of the H-like and He-like ions, reported as dashed lines, are much higher than expected, so that none of the H-like and He-like lines meet the common crossing point: observed fluxes are much higher than predicted. There are several possible explanations for such a behavior. The first one is that other processes than collisional excitation populate the upper levels in these ions. To investigate this, we included radiative recombination in the equations for level populations, using the rates provided by Mewe et al. (1995). The recombination rate increases with temperature because of the increasing H-like ion fractions so that inclusion of recombination is expected to be more important for lighter ions. While we found recombinations to be significant for Ne ix and Ne x lines, they do not account for the observed discrepancy. A second possibility is that, since the temperature of formation of the H-like and He-like ions whose lines were observed is much lower than the temperatures shown in Figure 4, lines from these ions are at least partially emitted by ambient active region plasma and not by the flare. However, the high density values indicated by some of these ions (see § 5.2) suggest that a significant portion of the fluxes of these lines is emitted by the flare. A comparison between fluxes of H-like and He-like lines with other flare measurements (McKenzie et al. 1980, 1982, 1985) and one active region observation (Parkinson

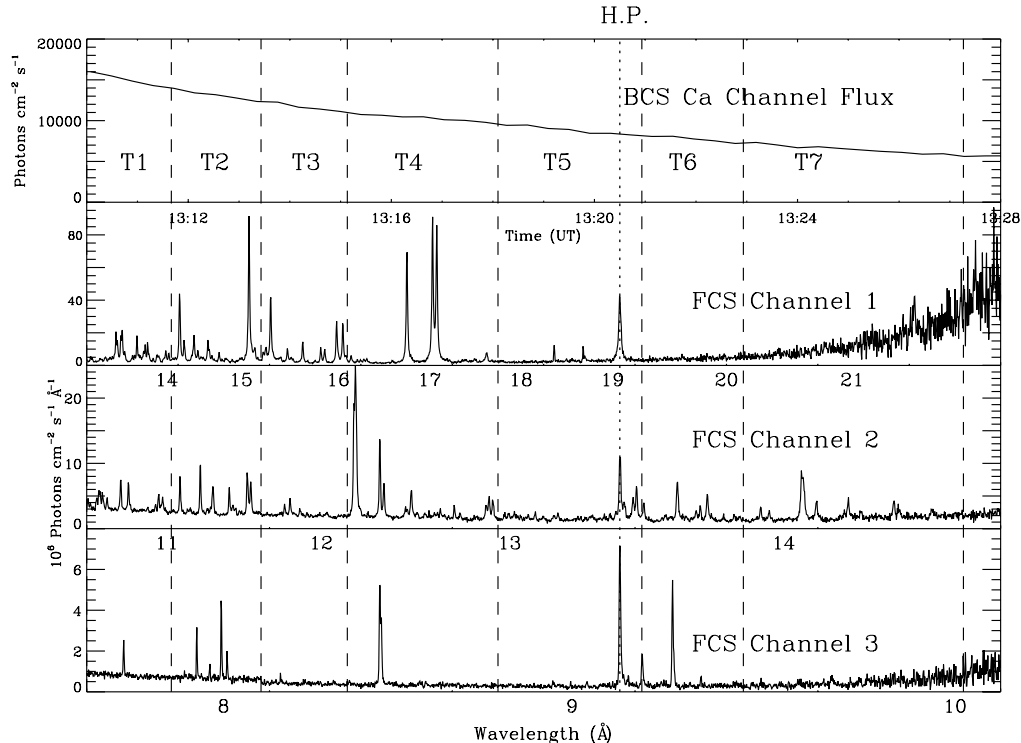


FIG. 3.—*Top panel*: Total flux in BCS Ca channel during the 1980 August 25 flare, with time (UT) shown on horizontal axis. T1, T2, . . . , T7, are the time bins as defined in this work (see Table 2 for exact time limits, which are shown as the dashed vertical lines). *Next three panels*: FCS spectral scans in channels 1, 2, and 3, with approximate wavelengths (Å) indicated on each horizontal axis; the FCS scanned in the direction of increasing wavelength as a function of time, with the wavelength scales adjusted so that the times of the top panel are consistent with the FCS scanning wavelengths. The dotted vertical line is the position of home position (H.P.) lines. Lines may be identified from Table 9.

1975) shows that the present fluxes are higher than active region ones but lower than other flares. Finally, the discrepancy might also be explained by the adopted coronal abundances from Feldman et al. (1992), which might be not representative of the emitting plasma. However, the correction to the abundances required to achieve agreement between Fe and Ni ions on one side, and H-like and He-like ions on the other, ranges from a factor of 3 to a factor of 15 and is different for each element; such a factor also seems to be dependent on time as different bins provide different corrections for the same element. These corrections are not consistent with photospheric abundances, as it could be expected if the flare plasma we are observing was produced by chromospheric evaporation.

These measurements allow the temporal behavior of the plasma to be determined and compared with results from the BCS observations described in §§ 5.3 and 5.5. The EM and T values measured from BCS and the EM analysis are displayed in Figures 5 and 6. Figure 6 shows that the EM determined from FCS lines decreases by a factor of about 6 in 10 minutes, while the EM determined from the Ca XIX w line and nearby continuum decreases by only a factor of 2.5 in the same time. The temperature variations have a smoother behavior: BCS values slowly decrease with time, while those from FCS are more scattered in the $\log T = 6.8-6.9$ range, although they show a slowly decreasing trend. In general, the temperature from the FCS lines is constant within 25%, while the BCS values slowly decrease by 20%.

The decrease of the FCS emission measure is faster than the BCS one, so that variations in line fluxes within each time bin can be larger than the 25% limit chosen for BCS fluxes to define the time bins. However, restricting the duration of each time bin

limits the number of lines from different ions in each time bin, so that the emission measure analysis would be much more uncertain or even impossible to carry out.

In order to verify the isothermality of the emitting source, we have performed a differential emission measure (DEM) analysis on the bin 1, channel 1 data set. Since the DEM curve indicates the distribution of plasma with temperature, nearly isothermal plasmas should show a very narrowly peaked curve. To determine the DEM on bin 1, channel 1, we have used the iterative procedure of Landi & Landini (1997). The ions available in that time bin are Fe XVII to Fe XX. The resulting DEM curve $\varphi(T)$ is shown in Figure 7. In the left panel, DEM measurements provided by each individual line are shown, at the effective temperature T_{eff} defined as

$$\log T_{\text{eff}} = \frac{\int \log TG(T)\varphi(T) dt}{\int G(T)\varphi(T) dt}, \quad (3)$$

where $G(T)$ is the contribution function of each line. We also have integrated the DEM curve in temperature with temperature steps of $\Delta(\log) = 0.05$ (T in K) in order to determine the temperature variation of the EM; in the right panel of Figure 7 we have shown the percentile contribution of each of the 0.05 temperature bins to the total value of the emission measure: 83% of the emission measure is concentrated in the $\log T = 6.8-7.0$ range. However, it is important to note that the smoothness assumption in the Landi & Landini (1997) method, as well as in the other DEM inversion techniques, tends to overestimate the DEM curve away from the peak when the DEM curve shows a very sharp maximum, so that the real DEM is likely to be even more peaked

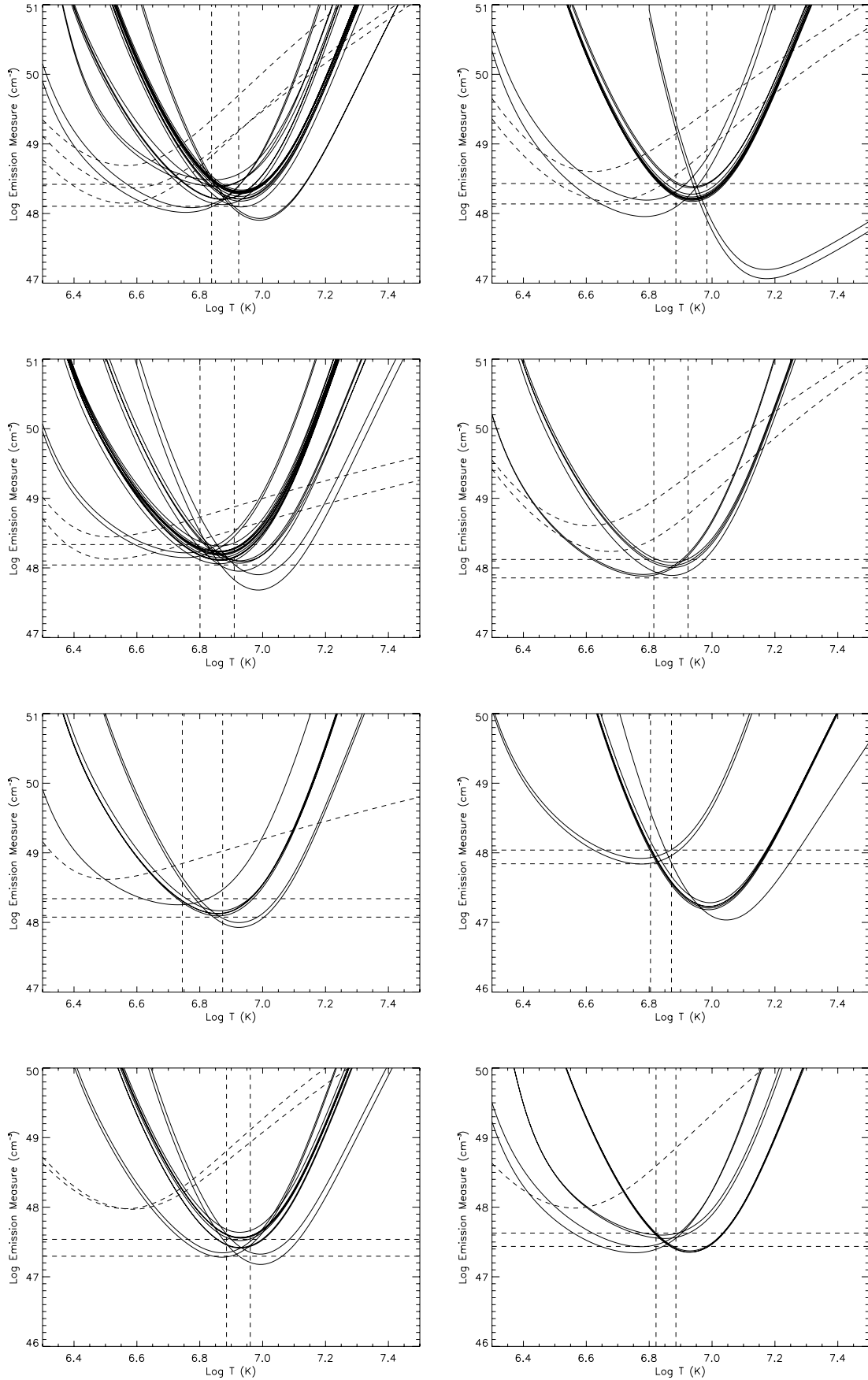


FIG. 4.—Results from the emission measure analysis. From top to bottom: *Left*: bin 1 (channel 1), *right*: bin 1 (channel 2); *Left*: bin 2 (channel 1), *right*: bin 2 (channel 2); *Left*: bin 3 (channel 2), *right*: bin 4 (channel 2); *Left*: bin 5 (channel 2), *right*: bin 6 (channel 2). The dotted lines show what is judged to be the common crossing point and the values of temperature and emission measure. Dashed correspond to the H-like and He-like lines in each bin.

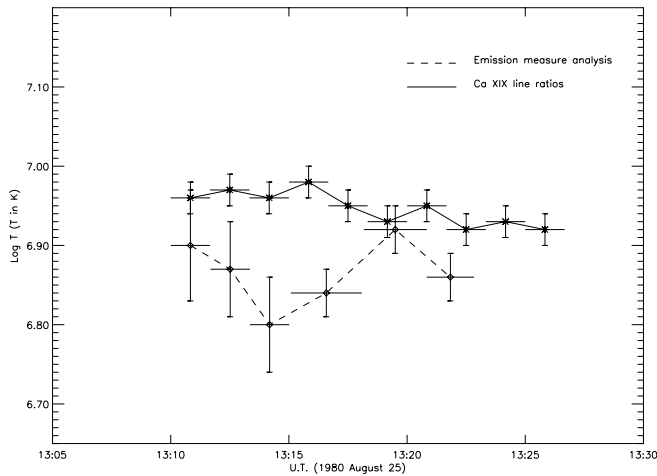


FIG. 5.—Temperature measurements as a function of time from the FCS and BCS observations. *Solid line*: Temperature from the Ca xviii *k* line/Ca xix *w* lines ratio BCS measurements for the 1980 August 25 flare. *Dashed line*: Temperature from the emission measure analysis of the FCS lines.

than the curve shown in Figure 7. This confirms the near isothermality of the plasma.

5.2. H-like and He-like Ion Line Ratio Diagnostics

Diagnostic results using H-like and He-like ions are listed in Tables 3 and 4. With only a few exceptions, the lines in each pair were observed within 100 s, so the ratios are unlikely to be affected by changes in the flare emission measure.

Electron temperatures could be measured both with H-like and He-like ions. For O viii and Ne x, lines from the Lyman series provide very sensitive temperature indicators. The measured temperatures are scattered in the $5.4 \leq \log T \leq 6.1$ range, and even lines within the Lyman series of the same ion provide different temperature values. However, all the measured values are well below the measured flare temperatures and the temperature of maximum abundance T_{\max} for those ions. The O viii measurements involving the 14.189 Å line provide unrealistically low temperatures. These values are probably due either to some problems in the rates involved in the formation of the 14.819 Å line, or in the weakness of the observed flux of this line. Temperatures from the He-like ions are higher than T_{\max} of each ion, but lower than the measured flare values. These results seem to confirm the fact that He-like and H-like ions are likely formed both by flare plasma and by the surrounding active region, as already shown by the EM analysis.

The electron density was measured from four different He-like ions, and it gives consistently lower limits for Ne ix and Na x, with densities lower than $1.5 \times 10^{11} \text{ cm}^{-3}$. During the last phase of the flare observations, a more precise measurement was possible, giving $10.7 \leq \log N_e \leq 11.3$ (N_e in cm^{-3}). While the lower limits are consistent with active region densities, the latter value is more typical of flares. In these measurements, we have assumed $T = T_{\max}$ for each ion. To assess the effect of the slight temperature dependence of these ratios, we have repeated the measurements assuming $\log T = 6.9$, as in the flare plasma and found a moderate 0.2 decrease in $\log N_e$. The Al xii measurement points to very high densities, much higher than densities expected for an M1.5 flares, and we suggest that some problem in the atomic physics or some blending line might be the cause of the high density. Using the CHIANTI database, we have checked the effects of the blending satellite lines to the

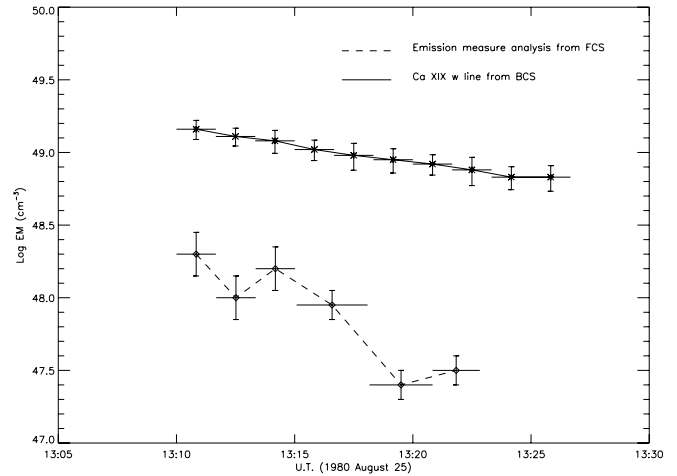


FIG. 6.—Emission measure from the Ca xix *w* line (*solid line*) derived from BCS measurements and from the emission measure analysis of FCS, channel 2 lines (*dashed line*), during the 1980 August 25 flare.

lines involved in the ratio. We have found that except for unrealistically low temperatures, the contribution of the satellites to the two lines is always smaller than 20%; moreover, their combined effect on the line ratio is even less.

5.3. Temperature from Ca xix Line Ratios

The temperature variations from the BCS Ca xix line emission and FCS emission measure analysis are shown in Figure 5. The BCS temperatures are slightly higher than those from the FCS analysis, possibly due to the larger BCS field of view including some hotter plasma. The temperature is very slowly decaying with time, decreasing from 9.1×10^6 to 8.3×10^6 K in 15 minutes. The decrease is very smooth, much smoother than the FCS temperatures, and it is nearly exponential with time to a first approximation. The uncertainties in the temperature are smaller than in the emission measure analysis because of the great temperature sensitivity of the Ca xix/Ca xviii (*k*) ratio.

5.4. Temperature from Dielectronic Satellite Lines

The temperature results from the ratios involving the dielectronic satellites lines (D) are given in Table 5. In that table, the notation introduced by Gabriel (1972), Bely-Dubau et al. (1979), and Dubau et al. (1981) is used to identify lines. The measured temperatures show a peculiar behavior. The Al xi(d)/Al xii and Mg x(d)/Mg xi ratios provide temperatures much lower than those measured using the EM analysis, and more typical of a nonflaring, hot active region. They seem to suggest that these ions are emitted by the surrounding active region and not by the flare plasma itself. By contrast, Mg xi(d)/Mg xii ratios indicate two different temperatures: the value of $\log T = 6.86 \pm 0.06$ is in excellent agreement with the results of the EM analysis, while the value $\log T = 7.05 \pm 0.08$ is too high. The former measurement seems to indicate that Mg xii lines are emitted by the flare plasma. These results are consistent with the fact that the Mg xii ion abundance peak at around 8–10 MK, very close to the temperature of the flare plasma, where Mg xi and Al xii ion abundances peak at lower temperatures (≈ 3 –4 MK), more typical of active regions. However, some caution should be used with these ratios, since the dielectronic lines observed during the 1980 August 25 are fairly weak. We also note that the July 2 temperature measurement from the

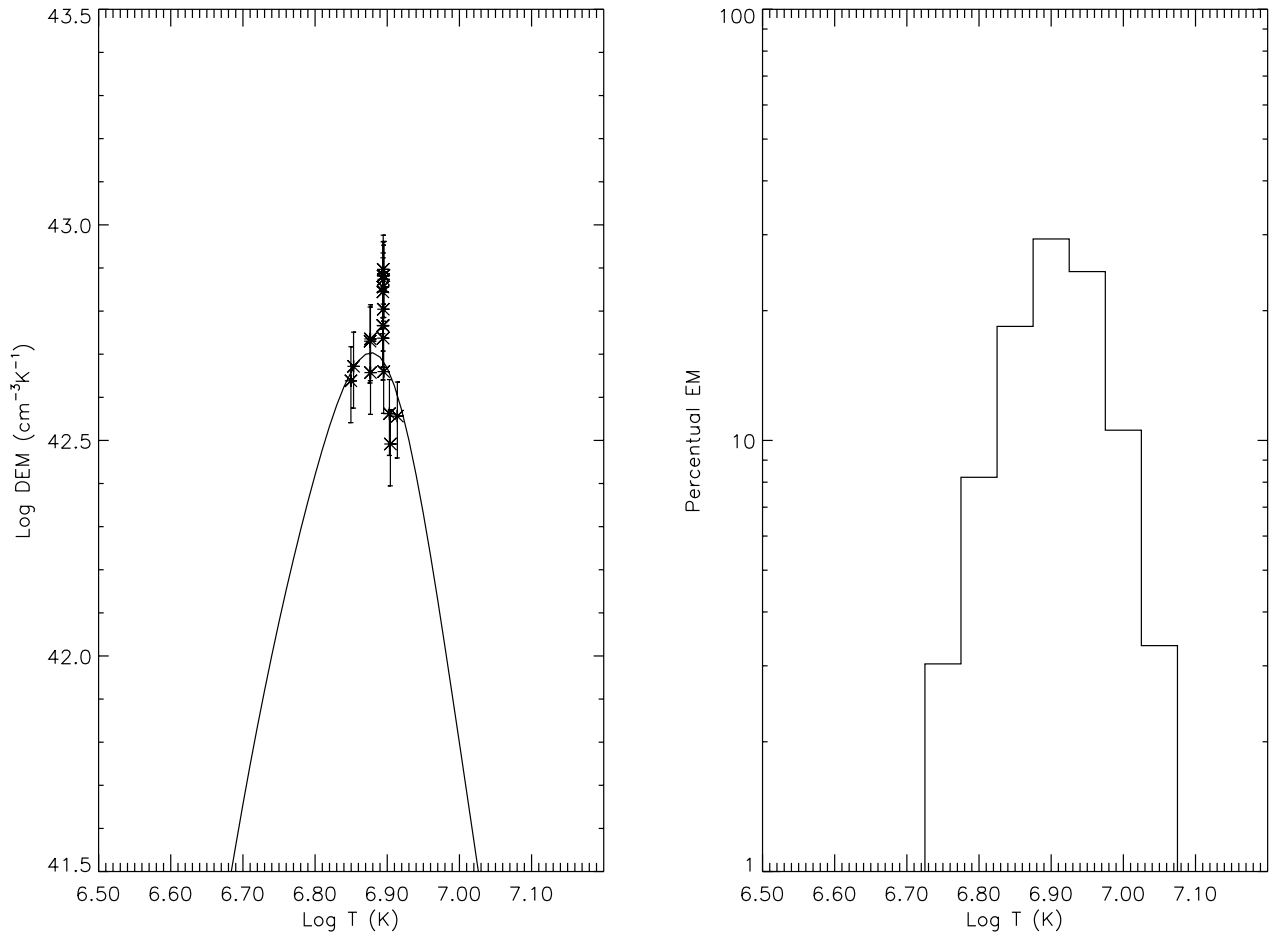


FIG. 7.—DEM determination for time bin 1, channel 1. *Left*: DEM curve obtained from Fe xvii to Fe xx fluxes. DEM values obtained from individual line fluxes are also shown. *Right*: Percentile contribution to the EM given by 0.05 log T intervals (see text).

Mg xi(d)/Mg xii ratio provides exceedingly high temperature (see § 6.2), but the dielectronic line is fairly weak also in that spectrum. In addition, there are several dielectronic satellite lines that blend the H-like Ly α and the w lines, but the measured temperatures in all cases are sufficiently high to limit the contributions from these unresolved satellites to within 10% of the measured flux, so that they are not the cause of the exceedingly high measured temperatures.

5.5. Emission Measure from BCS Line and Continuum Emission

The emission measure values obtained from the Ca xix w line as seen by BCS are shown in Figure 6. The emission measures from BCS line and continuum fluxes are equal within the uncertainties for all times. The emission measure of the plasma decreases steadily with time, changing by a factor ≈ 2.5 in

TABLE 3
ELECTRON DENSITY N_e (cm^{-3}) AND TEMPERATURE (T , IN K) ESTIMATES FROM He-LIKE LINE RATIOS DURING THE 1980 AUGUST 25 FLARE

ION	$\log T_{\max}$	Δt	Δt_{scan}	CHANNEL	$R = (x + y)/z$	$\log N_e$		$G = (x + y + z)/w$	$\log T$
						$\log T = \log T_{\max}$	$\log T = 6.9$		
Ne ix.....	6.2	45	23	1	0.37 ± 0.05	≤ 11.2	$11.4^{+0.2}_{-0.3}$	1.25 ± 0.12	6.00 ± 0.15
			13	1					
			620	2					
Na x.....	6.3	100	35	2	0.41 ± 0.05	$11.1^{+0.2}_{-0.4}$	$11.6^{+0.15}_{-0.25}$	0.38 ± 0.11^a	7.06 ± 0.15^a
			37	2					
			630	2					
Mg xi.....	6.4	610	57	3	0.44 ± 0.20	≤ 12.4	≤ 12.6	0.85 ± 0.05	6.59 ± 0.06
			33	3					
			620	3					
Al xii.....	6.5	125	33	3	0.37 ± 0.03	≤ 11.6	$12.0^{+0.25}_{-0.50}$	0.81 ± 0.06	6.76 ± 0.06
			19	3					
			135	3					
					0.49 ± 0.05	14.4 ± 0.2	$14.4^{+0.1}_{-0.15}$		

NOTE.—The variable Δt (in s) is the time since the start of the observation at 13:10:00 UT; Δt_{scan} (in s) is the time elapsed between the observation of the two lines in each ratio.

^a This ratio is underestimated due to a Ne ix blend to the Na x z line at 11.000 Å, leading to an overestimation of the temperature.

TABLE 4
TEMPERATURE T (IN K) ESTIMATES DURING THE 1980 AUGUST 25 FLARE USING LINE RATIOS FROM DIFFERENT COMPONENTS OF THE RYDBERG SERIES IN THE H-LIKE AND He-LIKE SEQUENCES

Ion	Δt	Line Ratio (λ in Å) ^a	R_{obs}	$\log T$	Δt_{scan}	Channel
H-like Ions						
O VIII.....	180	14.819/15.180	0.21 ± 0.05	5.42 ± 0.12	35	1
O VIII.....	240	14.819/16.007	0.043 ± 0.009	5.70 ± 0.07	116	1
O VIII.....	250	15.180/16.007	0.21 ± 0.03	5.95 ± 0.12	81	1
Ne X.....	†	9.482/12.131	0.0023 ± 0.0006	$6.11 \pm 0.04^*$	411	2, 3
Ne X.....	†	9.712/12.131	0.0070 ± 0.0015	$6.12 \pm 0.04^*$	516	2, 3
He-like Ions						
O VII.....	500	17.768/18.627	0.40 ± 0.15	≥ 6.10	92	1
Ne IX.....	60	10.764/11.000	0.23 ± 0.06^b	5.6 ± 0.2^b	43	2
Ne IX.....	130	11.000/11.547	0.53 ± 0.05	^{b,c}	102	2
Ne IX.....	140	10.764/11.547	0.12 ± 0.03	$6.6^{+0.8}_{-0.4}$	145	2
Mg XI.....	90	7.473/7.850	0.47 ± 0.03	^c	108	3
Mg XI.....	†	7.473/9.169	0.24 ± 0.02	^c	546	3
Mg XI.....	†	7.850/9.169	0.50 ± 0.03	^c	438	3

NOTES.—The variable Δt (in s) is the time since the start of the observation at 13:10:00 UT; Δt_{scan} (in s) is the time elapsed between the observation of the two lines in each ratio. A dagger (†) signifies that these ratios involve lines observed at very different times and in two different channels. An asterisk (*) signifies that, even assuming a factor of 2 error in the relative calibration of the two channels, the temperature is always $\log T \leq 6.3$ (T in K).

^a $(x + y)/w$ ratio for He-like ions, Lyman line ratios for H-like ions.

^b The Ne IX 11.000 Å is blended with a Na X line.

^c The observed ratio is higher than high-temperature limit for any density.

15 minutes. Note that the BCS field of view is much larger than the FCS one, and this explains the large difference between the BCS and the FCS-based emission measure values. The ratio of flare areas seen in the BCS and FCS fields of view is not easy to determine; in order to give an approximate estimate, we considered the flare emission in the FCS field of view (Fig. 1) done shortly before the FCS spectral scan. Estimating this area to be that of the brightest pixels in the O VIII, Ne IX, and Mg XI images, we found that the flare area in the BCS field of view is between 15 and 30 times the one observed by the FCS in its single pixel (14" square) during the spectral scan. This ratio is consistent with the factor of 10 difference in emission measures from the BCS and FCS.

The EM values obtained with the Ca XIX and the continuum flux could in principle lead to a determination of the absolute Ca abundance, but unfortunately at temperatures of $\approx 10^7$ K the continuum in the vicinity of 3 Å is due both to free-free radiation and to recombination continuum from Si. The relative importance of the two continua depends on the element abundances of the emitting plasma: at 10 MK, the recombination from Si accounts for 50% to 70% of the total emission.

5.6. Density and Temperature Diagnostics from Line Ratios of Iron Ions

Diagnostic results from line ratios from Fe lines are listed in Tables 6 and 7. The uncertainties in the observed fluxes are too

TABLE 5
TEMPERATURE ESTIMATES ($\log T$, T IN K) FROM RATIOS R_{obs} OF DIELECTRONIC SATELLITES (D) TO A DIRECT-EXCITATION LINE (w FOR He-LIKE IONS, $Ly\alpha$ FOR H-LIKE IONS) FOR LINES IN THE 1980 AUGUST 25 AND 1985 JULY 2 FLARES

Ions	Line Ratio	λ (Å)	Δt_{scan}	Δt	R_{obs}	$\log T$ (K)
1980 August 25						
Al XI(d)/Al XII.....	$(a1 + d13 + d15)/w$	7.775/7.757	5	115	0.079 ± 0.020	6.60 ± 0.06
Mg X(d)/Mg XI.....		8.070/7.850	65	170	0.105 ± 0.012	6.62 ± 0.03
Mg XI(d)/Mg XII.....	$(L3 + L61)/Ly\alpha$	8.408/(8.420+8.425)	4	315	0.024 ± 0.005	6.85 ± 0.06
	$9/Ly\alpha$	8.553/(8.420+8.425)	44	330	0.024 ± 0.007	7.04 ± 0.08
Mg X(d)/Mg XI.....	$(h15 + h16)/w$	9.180/9.169	4	585	0.076 ± 0.012	6.44 ± 0.04
	$(a1 + a2)/w$	9.189/9.169	7	585	0.029 ± 0.012	6.42 ± 0.10
	$(d5 + d13 + d15)/w$	9.193/9.169	9	585	0.056 ± 0.015	6.52 ± 0.07
	$(j + k + l)/w$	9.320/9.169	59	610	0.079 ± 0.018	6.52 ± 0.04
1985 July 2						
Mg XI(d)/Mg XII.....	$(1+4)/Ly\alpha$	8.523/(8.419+8.425)	43	250	0.011 ± 0.003	7.15 ± 0.08

NOTE.—The variable Δt (in s) is the time since the start of the observation at 13:10:00 UT (1980 August 25) and 21:10:00 UT (1985 July 2); Δt_{scan} (in s) is the time elapsed between the observation of the two lines in each ratio. Lines forming the ratios have been labeled using the notation first adopted by Gabriel (1972) and Bely-Dubau et al. (1979).

TABLE 6
ELECTRON DENSITY ESTIMATES $\log N_e$ (N_e IN cm^{-3}) FROM DENSITY-SENSITIVE Fe LINE PAIRS IN THE 1980 AUGUST 25 FCS SPECTRA

Ion	Ratio (λ in \AA)	Δt	Obs. Ratio	$\log N_e$	Channel	Notes
Fe XVIII.....	14.361/14.205	100	0.089 ± 0.012	≤ 13.0	1	
		800	0.049 ± 0.021	^a	2	14.361 \AA line weak
Fe XIX.....	13.462/13.525	40	0.60 ± 0.06	^b	1	
		600	0.64 ± 0.07	^b	2	
Fe XX.....	12.982/12.827	450	0.13 ± 0.04	≤ 13	2	
Fe XX.....	12.888/12.827	450	...	≤ 12	2	Otherwise 12.888 \AA is visible
Fe XXI.....	12.422/12.282	350	0.98 ± 0.08	^b	2	12.422 \AA line blended
Fe XXI.....	12.327/12.282	330	...	≤ 12	2	Otherwise 12.327 \AA is visible

NOTE.—The variable Δt (in s) is the time since the start of the observation at 13:10:00 UT.

^a The observed ratio is lower than predicted for any value of the electron density.

^b The observed ratio is higher than predicted for an value of the electron density.

TABLE 7
TEMPERATURE ESTIMATES FROM TEMPERATURE-SENSITIVE Fe LINE PAIRS IN THE 1980 AUGUST 25 FCS SPECTRA

Ion	Ratio (λ in \AA)	Δt	Obs. Ratio	$\log T$	Channel
Fe XVIII.....	13.355/14.204	80	0.021 ± 0.009	Any T	1
Fe XVIII.....	14.703/15.372	180	0.39 ± 0.16	≤ 6.7	1
Fe XVIII.....	14.703/15.627	190	0.065 ± 0.020	6.7 ± 0.25	1
Fe XVIII.....	16.309/15.830	270	0.27 ± 0.04	≥ 6.6	1
Fe XIX.....	13.018/13.466	540	0.23 ± 0.05	≥ 6.7	2
Fe XX.....	12.581/12.827	330	0.28 ± 0.04	≥ 7.1	2
Fe XX.....	13.052/13.405	530	1.78 ± 0.47	^a	2

NOTE.—The variable Δt (in s) is the time since the start of the observation at 13:10:00 UT.

^a The observed ratio is higher than predicted for any value of the electron temperature.

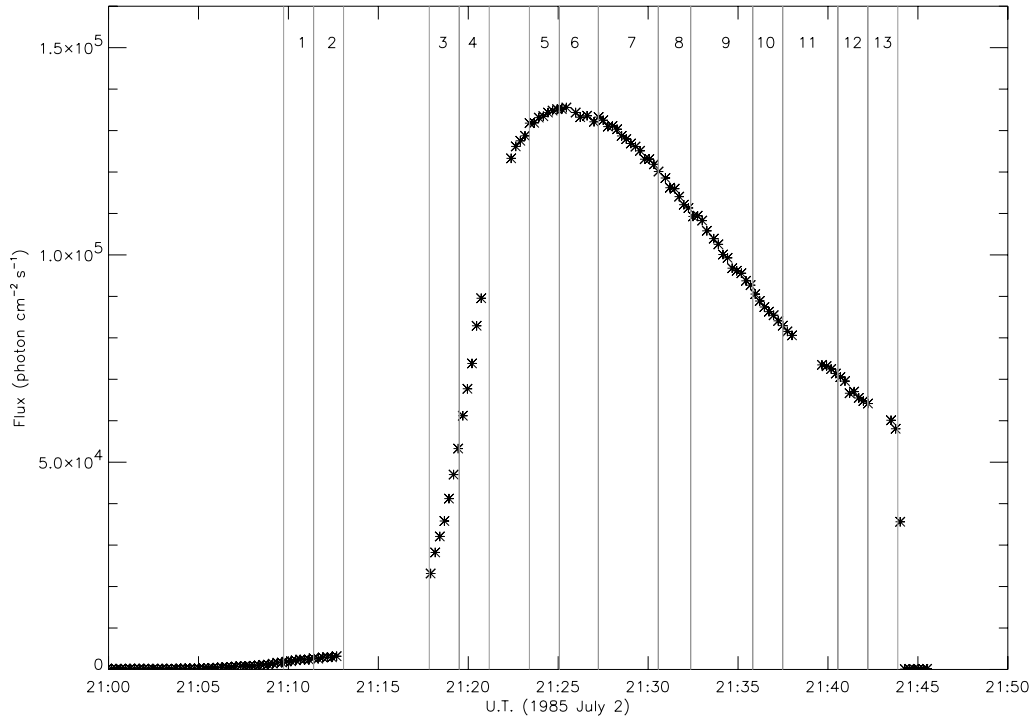


FIG. 8.—Total BCS Ca XIX channel flux as a function of time during the 1985 July 2 flare. The time bins correspond to the FCS analysis (see § 6).

high to allow a detailed plasma diagnostics to be carried out, since the error bars are of the same order of the temperature dependence of the ratio. The density diagnostic line ratios are all consistent in indicating an upper limit to the electron density, which is smaller than 10^{12} cm^{-3} , as indicated by the Fe xx and Fe xxI ratios. As noted by Phillips et al. (1982), some of the ratios involve an unobserved line; these are given since the latter line is strongly density sensitive and its absence from the observed spectrum is an indication that the electron density does not exceed 10^{12} cm^{-3} . This limit is consistent with the density of a moderate (M-class) flare in declining phase and with the measurements from the He-like ions. A few line ratios do not agree with the observations for any temperature or density, but this is due either to unresolved blends or to the weakness of one of the lines in the ratio. We note that the inclusion of collisional resonances and recombination in the level population calculation for Fe xvii, as described by Gu (2003), causes the relative emissivities from this ion to be density insensitive.

6. RESULTS: 1985 JULY 2 FLARE

6.1. Temperature from Ca xix Line Ratios

To measure the electron temperature and the emission measure during the 1985 July 2 flare, we divided the time period of observations into 13 time bins of unequal length, choosing the duration of each bin such that there was a minimum variation in the BCS Ca xix channel flux (see Fig. 8). Even so, the flux rose by a factor of 2 over the period of time bins 3 and 4.

The electron temperature derived from the ratio of the Ca xviii *k* dielectronic satellite to the Ca xix resonance line in BCS spectra is shown in Figure 9. A rise to a maximum, which is about 5 minutes earlier than the BCS Ca channel flux maximum (Fig. 8), is observed for this flare.

6.2. Temperature from Dielectronic Satellite Lines

Table 5 gives the temperature measured from the Mg xi(d)/Mg xii ratio, the only dielectronic satellite/direct excitation line ratio available in the 1985 July 2 data set. It is significantly higher than those obtained with the Ca xix line ratios. This is probably due to the weakness of the Mg xi(d) line.

6.3. Diagnostics from Line Ratios of Iron Ions

Fawcett et al. (1987) and Phillips et al. (1996) were the first to demonstrate the availability of density sensitive line ratios

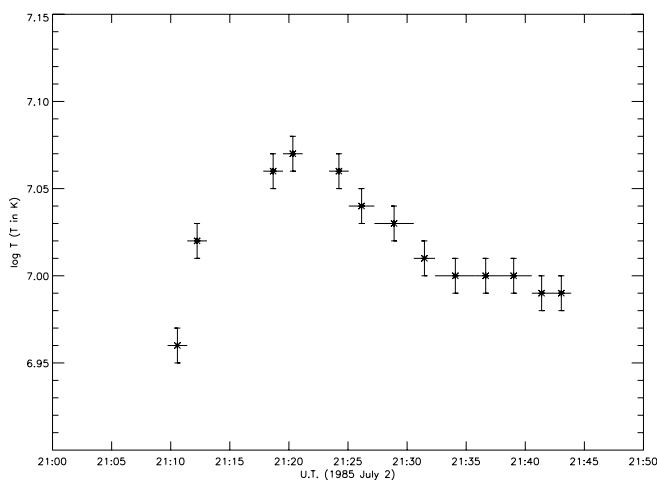


FIG. 9.—Temperature measurements as a function of time from the Ca xviii *k* line/Ca xix *w* line ratio measurements for the 1985 July 2 flare.

TABLE 8
ELECTRON DENSITY $\log N_e$ (N_e IN cm^{-3}) MEASUREMENTS
FROM THE 1985 JULY 2 DATA SET

Ion	Lines	Δt_{scan}	R_{obs}	$\log N_e$
Fe xxI	9.547/9.476	39	0.40 ± 0.04	13.1 ± 0.3
	9.806/9.547	157	0.27 ± 0.04	13.5 ± 0.15
	9.973/9.547	201	0.22 ± 0.04	13.3 ± 0.2
Fe xxII	9.075/8.976	47	0.39 ± 0.02	≤ 12.0
	8.090/9.075	432	0.24 ± 0.12	≥ 13.0
	8.715/9.075	164	0.42 ± 0.03	13.0 ± 0.15
	9.241/9.075	88	0.42 ± 0.07	13.1 ± 0.2

NOTE.—The variable Δt_{scan} (in s) is the time elapsed between the observation of the two lines in each ratio.

in the 7.4–10 Å spectral range from Fe xxI and Fe xxII. These ratios are very useful as they allow the determination of flare electron density at very high temperatures ($\approx 10^7$ K). In both these works, the July 2 data set was analyzed, and densities were determined by comparison with theoretical estimates obtained using distorted wave transition rates.

We remeasured the Fe xxI and Fe xxII line fluxes and used them to obtain ratios that can be compared with theoretical ratios from CHIANTI. The results are given in Table 8. We include only lines that are considered strong enough to give reliable ratios. The 9.547 and 9.476 Å lines are particularly strong and were scanned over a short period of time, so the density measurement from the ratio of these two lines should be the most sound. The 9.806 and 9.973 Å lines were scanned 2 or 3 minutes after these lines. Our estimate of N_e from the 9.547/9.476 Å ratio, of order 10^{13} cm^{-3} , is similar to, though slightly higher than, that obtained by Phillips et al. (1996). The difference may in part be due to the neglect of Fe xxI configurations involving $n = 3$ electrons in the model used by Phillips et al. (1996). Some of the Fe xxII line ratios give similarly high values of N_e , but not the 9.075/8.976 Å ratio.

6.4. H-like and He-like Ion Line Diagnostics

Given the short wavelength range covered by the July 2 spectral scan, only very few H-like and He-like diagnostic ratios can be found. Also, since the flare has a higher GOES class

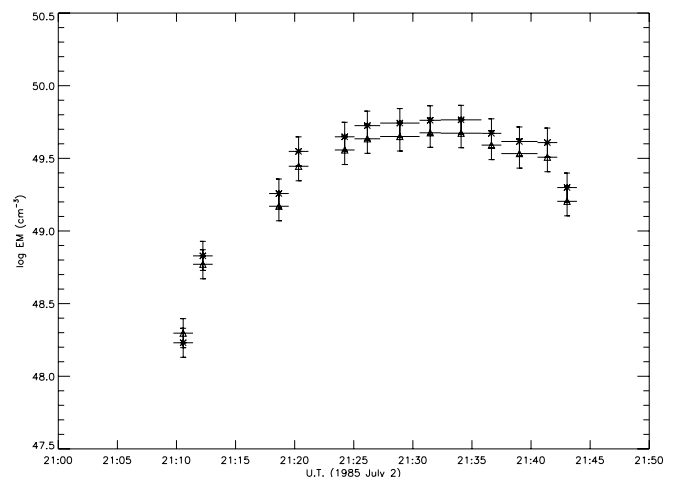


FIG. 10.—Emission measure measurements from BCS line ratio as a function of time from the 1985 July 2 flare spectrum. Emission measure was obtained from the Ca xix *w* line flux (stars) and the continuum (triangles).

TABLE 9
LINE LIST COMPILED FROM THE 1980 AUGUST 25 FCS SPECTRA

TIME	ION	λ_{pred}	TRANSITION	CHANNEL 1		CHANNEL 2		CHANNEL 3	
				λ_{obs}	Flux	λ_{obs}	Flux	λ_{obs}	Flux
Time Bin 1									
4.....	Fe xviii	10.580	$2s^2 2p^5 2P_{3/2}-2s 2p^5 (3P) 4p 2P_{3/2}$			10.580	7.1 ± 1.4		
	Fe xviii	10.580	$2s^2 2p^5 2P_{3/2}-2s 2p^5 (3P) 4p 2D_{5/2}$						
	Fe xviii	10.578	$2s^2 2p^5 2P_{3/2}-2s 2p^5 (3P) 4p 4P_{5/2}$						
	Fe xviii	10.587	$2s^2 2p^5 2P_{3/2}-2s^2 2p^4 (3P) 5s 4P_{1/2}$						
4.....	Fe xx	13.141	$2s^2 2p^3 2D_{3/2}-2s^2 2p^2 (3P) 3d 2F_{5/2}$	13.142	44.1 ± 5.1				
	Fe xx	13.143	$2s^2 2p^3 2D_{5/2}-2s^2 2p^2 (3P) 3d 4P_{5/2}$						
	Fe xvii	13.135	$2s^2 2p^6 1S_0-2s 2p^6 3d 1D_2$						
6.....				13.162	29.2 ± 4.2				
11.....						10.619	16.2 ± 1.5		
13.....	Fe xix	10.632	$2s^2 2p^4 3P_0-2s^2 2p^3 (2P) 4d 3D_1$			10.632	23.8 ± 2.1		
	Fe xix	10.632	$2s^2 2p^4 3P_2-2s^2 2p^3 (2D) 4d 3S_1$						
14.....	Fe xix	13.254	$2s^2 2p^4 3P_2-2s^2 2p^3 (2P) 3d 3D_3$	13.254	24.8 ± 4.9				
	Fe xx	13.254	$2s^2 2p^3 2P_{1/2}-2s^2 2p^2 (3P) 3d 4P_{1/2}$						
	Ni xx	13.256	$2s^2 2p^5 2P_{3/2}-2p^4 (3P) 3s 2P_{3/2}$						
	Fe xxi	13.252	$2s^2 2p^2 3P_2-2s^2 2p 3s 3P_1$						
14.....	Fe xix	10.641	$2s^2 2p^4 3P_2-2s^2 2p^3 (2D) 4d 3P_2$			10.641	21.0 ± 2.0		
	Fe xviii	10.640	$2s^2 2p^5 2P_{1/2}-2s^2 2p^4 (3P) 5d 2D_{3/2}$						
15.....	Fe xx	13.267	$2s^2 2p^3 2P_{1/2}-2s^2 2p^2 (3P) 3d 2P_{1/2}$	13.267	16.1 ± 4.6				
	Fe xx	13.267	$2s^2 2p^3 2D_{5/2}-2s^2 2p^2 (3P) 3d 4F_{7/2}$						
	Fe xx	13.269	$2s^2 2p^3 2D_{5/2}-2s^2 2p^2 (3P) 3d 2P_{3/2}$						
17.....				13.281	16.2 ± 4.3				
17.....	Fe xix	10.655	$2s^2 2p^4 3P_2-2s^2 2p^3 (2D) 4d 3D_3$			10.655	20.6 ± 1.9		
	Fe xvii	10.658	$2s^2 2p^6 1S_0-2s^2 2p^5 6d 3D_1$						
18.....						10.663	7.6 ± 1.7		
19.....	Ni xx	13.309	$2s^2 2p^5 2P_{3/2}-2p^4 (3P) 3s 4P_{5/2}$	13.312	29.2 ± 4.7				
	Fe xix	13.314	$2s 2p^5 3P_2-2s 2p^4 (2P) 3d 3D_3$						
21.....	Fe xx	13.327	$2s^2 2p^3 4S_{3/2}-2s^2 2p^2 (3P) 3p 4D_{7/2}$	13.326	37.7 ± 5.1				
	Fe xx	13.333	$2s^2 2p^3 2D_{3/2}-2s^2 2p^2 (3P) 3d 4F_{3/2}$						
	Fe xviii	13.326	$2s^2 2p^5 2P_{3/2}-2s 2p^5 (3P) 3p 4P_{5/2}$						
	Fe xviii	13.326	$2s^2 2p^5 2P_{3/2}-2s 2p^5 (3P) 3p 2P_{1/2}$						
22.....	Fe xix	10.684	$2s^2 2p^4 3P_2-2s^2 2p^3 (2D) 4d 3F_3$			10.684	15.0 ± 1.5		
24.....	Fe xviii	13.355	$2s^2 2p^5 2P_{3/2}-2s 2p^5 (3P) 3p 2P_{3/2}$	13.359	17.2 ± 7.3				
25.....	Fe xviii	13.378	$2s^2 2p^5 2P_{3/2}-2s 2p^5 (3P) 3p 2D_{5/2}$	13.378	34.7 ± 7.9				
28.....	Fe xx	13.405	$2s 2p^4 4P_{5/2}-2s 2p^3 (3S) 3d 4D_{7/2}$	13.405	42.7 ± 8.0				
	Fe xviii	13.405	$2s^2 2p^5 2P_{3/2}-2s 2p^5 (3P) 3p 4D_{3/2}$						
30.....	Fe xix	13.430	$2s^2 2p^4 3P_2-2s^2 2p^3 (2D) 3d 1F_3$	13.429	60.9 ± 8.9				
32.....	Ne ix	13.447	$1s^2 1S_0-1s 2p 1P_1$	13.448	258.4 ± 18.0				
	Fe xviii	13.448	$2s^2 2p^5 2P_{3/2}-2s 2p^5 (3P) 3p 4D_{5/2}$						
34.....	Fe xix	13.456	$2s^2 2p^4 3P_2-2s^2 2p^3 (2D) 3d 3S_1$	13.466	177.3 ± 14.6				
	Fe xix	13.462	$2s^2 2p^4 3P_0-2s^2 2p^3 (2P) 3d 3P_1$						
35.....				13.484	47.6 ± 6.9				
35.....	Mg xi	7.473	$1s^2 1S_0-1s 4p 1P_1$					7.473	8.1 ± 0.5
36.....	Ne ix	10.764	$1s^2 1S_0-1s 5p 1P_1$			10.760	6.0 ± 1.4		
	Fe xix	10.760	$2s^2 2p^4 3P_1-2s^2 2p^3 (2D) 4d 3D_2$						
	Fe xix	10.760	$2s^2 2p^4 3P_1-2s^2 2p^3 (2D) 4d 3P_1$						
37.....	Fe xvii	10.770	$2s^2 2p^6 1S_0-2s^2 2p^5 6d 1P_1$			10.769	40.4 ± 2.1		
37.....	Fe xix	13.506	$2s^2 2p^4 3P_2-2s^2 2p^3 (2D) 3d 3D_2$	13.506	222.0 ± 16.3				
	Fe xx	13.505	$2s 2p^4 4P_{3/2}-2s 2p^3 (3S) 3d 4D_{3/2}$						
	Fe xxi	13.507	$2s 2p^3 3D_1-2s 2p^2 (4P) 3s 3P_0$						
39.....	Fe xix	13.525	$2s^2 2p^4 3P_2-2s^2 2p^3 (2D) 3d 3D_3$	13.522	296.9 ± 19.0				
39.....						10.781	3.1 ± 1.0		
40.....				13.540	57.3 ± 9.9				
42.....	Ne ix	13.553	$1s^2 1S_0-1s 2p 3P_1$	13.555	87.6 ± 9.8				
	Fe xix	13.555	$2s^2 2p^4 3P_2-2s^2 2p^3 (2D) 3d 3P_2$						
	Fe xix	13.550	$2s^2 2p^4 3P_2-2s^2 2p^3 (2D) 3d 1P_1$						
44.....	Fe xix	10.805	$2s^2 2p^4 1D_2-2s^2 2p^3 (2D) 4d 1F_3$			10.805	4.3 ± 1.0		
	Fe xix	10.805	$2s^2 2p^4 3P_1-2s^2 2p^3 (2D) 4d 3F_2$						
46.....	Fe xix	10.816	$2s^2 2p^4 3P_2-2s^2 2p^3 (4S) 4d 3D_3$			10.816	36.3 ± 1.9		
48.....	Fe xix	10.827	$2s^2 2p^4 1D_2-2s^2 2p^3 (2D) 4d 3S_1$			10.827	6.9 ± 1.1		
	Fe xix	10.827	$2s^2 2p^4 3P_2-2s^2 2p^3 (4S) 4d 3D_2$						
	Fe xix	10.825	$2s^2 2p^4 1D_2-2s^2 2p^3 (2D) 4d 1D_2$						

TABLE 9—Continued

TIME	ION	λ_{pred}	TRANSITION	CHANNEL 1		CHANNEL 2		CHANNEL 3	
				λ_{obs}	Flux	λ_{obs}	Flux	λ_{obs}	Flux
49.....	Fe XIX	13.636	$2s^2 2p^4 {}^3P_2-2s^2 2p^3 ({}^2D) 3d {}^3G_3$	13.631	17.7 ± 5.3				
50.....	Fe XIX	13.648	$2s^2 2p^4 {}^3P_2-2s^2 2p^3 ({}^2D) 3d {}^3F_3$	13.648	57.9 ± 6.5				
53.....	Fe XIX	13.672	$2s^2 2p^4 {}^3P_1-2s^2 2p^3 ({}^2D) 3d {}^3D_2$	13.672	64.8 ± 6.1				
	Fe XIX	13.672	$2s^2 2p^4 {}^3P_1-2s^2 2p^3 ({}^2D) 3d {}^3P_1$						
	Fe XIX	13.673	$2s^2 2p^4 {}^3P_2-2s^2 2p^3 ({}^2D) 3d {}^3F_2$						
55.....	Ne IX	13.699	$1s^2 {}^1S_0-1s 2s {}^3S_1$	13.700	235.3 ± 11.9				
57.....	Fe XIX	13.721	$2s^2 2p^4 {}^3P_1-2s^2 2p^3 ({}^2D) 3d {}^3P_2$	13.721	64.5 ± 6.4				
	Fe XIX	13.721	$2s^2 2p^4 {}^1D_2-2s^2 2p^3 ({}^2P) 3d {}^3F_3$						
59.....	Fe XIX	13.741	$2s^2 2p^4 {}^1D_2-2s^2 2p^3 ({}^2D) 3d {}^1F_3$	13.742	57.7 ± 5.9				
61.....	Fe XIX	13.762	$2s^2 2p^4 {}^3P_0-2s^2 2p^3 ({}^2D) 3d {}^3D_1$	13.762	37.0 ± 6.4				
	Fe XIX	13.769	$2s^2 2p^4 {}^1D_2-2s^2 2p^3 ({}^2D) 3d {}^3S_1$						
62.....	Ni XIX	13.779	$2p^6 {}^1S_0-2p^5 3s {}^1P_1$	13.780	96.8 ± 8.7				
	Fe XX	13.781	$2s^2 2p^3 {}^4S_{3/2}-2s^2 2p^2 ({}^3P) 3s {}^4P_{5/2}$						
64.....	Fe XIX	13.799	$2s^2 2p^4 {}^3P_2-2s^2 2p^3 ({}^4S) 3d {}^3D_3$	13.799	145.9 ± 10.3				
67.....	Fe XVII	13.823	$2s^2 2p^6 {}^1S_0-2s 2p^6 3p {}^1P_1$	13.826	171.1 ± 11.3				
67.....	Fe XIX	10.933	$2s^2 2p^4 {}^3P_1-2s^2 2p^3 ({}^4S) 4d {}^3D_2$			10.933	5.2 ± 1.1		
	Fe XIX	10.936	$2s^2 2p^4 {}^3P_1-2s^2 2p^3 ({}^4S) 4d {}^3D_1$						
68.....	Fe XIX	13.844	$2s^2 2p^4 {}^3P_2-2s^2 2p^3 ({}^4S) 3d {}^3D_2$	13.844	64.1 ± 7.5				
	Fe XX	13.844	$2s^2 2p^3 {}^4S_{3/2}-2s^2 2p^2 ({}^3P) 3s {}^4P_{3/2}$						
	Fe XIX	13.841	$2s^2 2p^4 {}^1D_2-2s^2 2p^3 ({}^2D) 3d {}^3D_3$						
	Fe XIX	13.843	$2s^2 2p^4 {}^3P_1-2s^2 2p^3 ({}^2D) 3d {}^3F_2$						
73.....	Fe XVII	13.891	$2s^2 2p^6 {}^1S_0-2s 2p^6 3p {}^3P_1$	13.892	27.2 ± 5.8				
76.....	Fe XXIII	10.981	$2s^2 {}^1S_0-2s 3p {}^1P_1$			10.981	10.4 ± 1.3		
	Fe XIX	10.981	$2s 2p^5 {}^3P_2-2s 2p^4 ({}^4P) 4d {}^5F_3$						
	Fe XIX	10.981	$2s 2p^5 {}^3P_2-2s 2p^4 ({}^4P) 4d {}^5P_2$						
77.....	Fe XIX	13.936	$2s^2 2p^4 {}^3P_0-2s^2 2p^3 ({}^4S) 3d {}^3D_1$	13.938	87.8 ± 14.9				
	Fe XIX	13.938	$2s^2 2p^4 {}^3P_2-2s^2 2p^3 ({}^4S) 3d {}^5D_3$						
	Fe XIX	13.938	$2s^2 2p^4 {}^3P_2-2s^2 2p^3 ({}^4S) 3d {}^5D_1$						
	Fe XIX	13.938	$2s^2 2p^4 {}^3P_2-2s^2 2p^3 ({}^4S) 3d {}^5D_2$						
	Fe XIX	13.938	$2s 2p^5 {}^3P_2-2s 2p^4 ({}^4P) 3d {}^3D_3$						
79.....	Ne IX	11.000	$1s^2 {}^1S_0-1s 4p {}^1P_1$			11.000	25.9 ± 1.9		
	Na X	11.003	$1s^2 {}^1S_0-1s 2p {}^1P_1$						
79.....	Fe XVIII	13.962	$2s^2 2p^5 {}^2P_{3/2}-2s^2 2p^4 ({}^1S) 3d {}^2D_{5/2}$	13.962	75.5 ± 14.1				
	Fe XIX	13.957	$2s^2 2p^4 {}^1D_2-2s^2 2p^3 ({}^2D) 3d {}^3G_3$						
	Fe XIX	13.962	$2s 2p^5 {}^3P_2-2s 2p^4 ({}^4P) 3d {}^3F_2$						
	Fe XIX	13.964	$2s^2 2p^4 {}^3P_1-2s^2 2p^3 ({}^4S) 3d {}^3D_1$						
82.....	Fe XXIII	11.019	$2s^2 {}^1S_0-2s 3p {}^3P_1$			11.014	9.4 ± 1.4		
84.....	Fe XVII	11.023	$2s^2 2p^6 {}^1S_0-2s 2p^6 4p {}^1P_1$			11.025	20.1 ± 1.7		
85.....	Fe XIX	14.017	$2s^2 2p^4 {}^3P_1-2s^2 2p^3 ({}^4S) 3d {}^3D_2$	14.017	37.8 ± 11.6				
	Fe XIX	14.017	$2s 2p^5 {}^3P_1-2s 2p^4 ({}^4P) 3d {}^3P_2$						
	Fe XXI	14.008	$2s 2p^3 {}^3D_1-2s^2 2p 3p {}^3P_0$						
86.....	Fe XVII	11.043	$2s^2 2p^6 {}^1S_0-2s 2p^6 4p {}^3P_1$			11.040	4.3 ± 1.1		
87.....	Ni XIX	14.043	$2p^6 {}^1S_0-2p^5 3s {}^3P_1$	14.042	119.7 ± 14.8				
	Fe XIX	14.042	$2s 2p^5 {}^3P_2-2s 2p^4 ({}^4P) 3d {}^3F_3$						
	Fe XIX	14.043	$2s 2p^5 {}^3P_2-2s 2p^4 ({}^4P) 3d {}^3D_2$						
90.....	Ni XIX	14.077	$2p^6 {}^1S_0-2p^5 3s {}^3P_2$	14.078	88.6 ± 13.0				
95.....	Fe XVIII	14.125	$2s^2 2p^5 {}^2P_{1/2}-2s^2 2p^4 ({}^1S) 3d {}^2D_{3/2}$	14.125	34.8 ± 10.8				
	Fe XX	14.123	$2s^2 2p^3 {}^2D_{5/2}-2s^2 2p^2 ({}^3P) 3s {}^4P_{5/2}$						
95.....	Na X	11.083	$1s^2 {}^1S_0-1s 2p {}^3P_1$			11.088	3.0 ± 1.1		
98.....	Fe XVIII	14.155	$2s^2 2p^5 {}^2P_{3/2}-2s^2 2p^4 ({}^1D) 3d {}^2D_{3/2}$	14.156	39.6 ± 11.0				
Time Bin 2									
102.....	Fe XVIII	14.206	$2s^2 2p^5 {}^2P_{3/2}-2s^2 2p^4 ({}^1D) 3d {}^2D_{5/2}$	14.206	835.3 ± 40.7				
	Fe XVIII	14.209	$2s^2 2p^5 {}^2P_{3/2}-2s^2 2p^4 ({}^1D) 3d {}^2P_{3/2}$						
103.....	Fe XVII	11.133	$2s^2 2p^6 {}^1S_0-2s^2 2p^5 5d {}^1P_1$			11.129	47.8 ± 3.0		
107.....	Fe XVIII	14.258	$2s^2 2p^5 {}^2P_{3/2}-2s^2 2p^4 ({}^1D) 3d {}^2S_{1/2}$	14.259	232.0 ± 18.6				
	Fe XVIII	14.259	$2s^2 2p^5 {}^2P_{3/2}-2s^2 2p^4 ({}^1D) 3d {}^2F_{5/2}$						
	Fe XX	14.263	$2s 2p^4 {}^4P_{5/2}-2s 2p^3 ({}^3S) 3s {}^4S_{3/2}$						
111.....	Fe XVIII	11.162	$2s^2 2p^5 {}^2P_{3/2}-2s^2 2p^4 ({}^1S) 4d {}^2D_{5/2}$			11.174	4.3 ± 1.7		
114.....	Na X	11.192	$1s^2 {}^1S_0-1s 2s {}^3S_1$			11.190	6.8 ± 1.7		
115.....	Fe XVIII	14.340	$2s^2 2p^5 {}^2P_{1/2}-2s^2 2p^4 ({}^1D) 3d {}^2P_{1/2}$	14.346	37.1 ± 5.6				
116.....	Al XII	7.757	$1s^2 {}^1S_0-1s 2p {}^1P_1$					7.757	10.1 ± 0.4
117.....	Fe XVIII	14.363	$2s^2 2p^5 {}^2P_{1/2}-2s^2 2p^4 ({}^1D) 3d {}^2D_{3/2}$	14.362	74.0 ± 9.1				

TABLE 9—Continued

TIME	ION	λ_{pred}	TRANSITION	CHANNEL 1		CHANNEL 2		CHANNEL 3	
				λ_{obs}	Flux	λ_{obs}	Flux	λ_{obs}	Flux
118.....	Fe XVIII	14.376	$2s^2 2p^5 2P_{3/2}-2s^2 2p^4 ({}^3P) 3d {}^2D_{5/2}$	14.376	204.2 \pm 13.2				
119.....				14.389	32.8 \pm 7.0				
121.....	Al XI (d)	7.778	$1s^2 3p {}^2P_{3/2}-1s 2p ({}^1P) 3p {}^2D_{5/2}$					7.775	0.8 \pm 0.2
	Al XI (d)	7.777	$1s^2 3p {}^2P_{1/2}-1s 2p ({}^1P) 3p {}^2D_{3/2}$						
	Al XI (d)	7.774	$1s^2 3s {}^2S_{1/2}-1s 2p ({}^1P) 3s {}^2P_{3/2}$						
121.....	Fe XX	14.403	$2s 2p^4 {}^4P_{3/2}-2s 2p^3 ({}^5S) 3s {}^4S_{3/2}$	14.403	24.8 \pm 4.8				
122.....	Fe XVIII	14.419	$2s^2 2p^5 2P_{1/2}-2s^2 2p^4 ({}^1D) 3d {}^2P_{3/2}$	14.421	91.7 \pm 7.2				
	Fe XVIII	14.421	$2s^2 2p^5 2P_{3/2}-2s^2 2p^4 ({}^3P) 3d {}^4P_{3/2}$						
125.....	Fe XVII	11.253	$2s^2 2p^6 {}^1S_0-2s^2 2p^5 5d {}^3D_1$			11.250	65.2 \pm 3.6		
125.....	Fe XVIII	14.452	$2s^2 2p^5 2P_{3/2}-2s^2 2p^4 ({}^3P) 3d {}^2D_{3/2}$	14.453	26.1 \pm 5.0				
	Fe XX	14.449	$2p^4 {}^4P_{1/2}-2s 2p^3 ({}^5S) 3s {}^4S_{3/2}$						
	Fe XX	14.453	$2s 2p^4 {}^4P_{3/2}-2s^2 2p^2 ({}^1D) 3p {}^2P_{3/2}$						
127.....	Fe XVIII	14.470	$2s^2 2p^5 2P_{1/2}-2s^2 2p^4 ({}^1D) 3d {}^2S_{1/2}$	14.468	25.1 \pm 5.0				
129.....	Fe XVIII	14.486	$2s^2 2p^5 2P_{3/2}-2s^2 2p^4 ({}^3P) 3d {}^4F_{3/2}$	14.486	23.0 \pm 4.5				
130.....	Al XII	7.807	$1s^2 {}^1S_0-1s 2p {}^3P_1$					7.807	2.7 \pm 0.2
133.....	Fe XVII	11.287	$2s^2 2p^6 {}^1S_0-2s^2 2p^5 5s {}^3P_1$			11.292	7.7 \pm 1.7		
	Fe XIX	11.292	$2s 2p^5 {}^3P_2-2s 2p^4 ({}^4P) 4s {}^3P_2$						
133.....	Fe XVIII	14.537	$2s^2 2p^5 2P_{3/2}-2s^2 2p^4 ({}^3P) 3d {}^2F_{5/2}$	14.537	209.9 \pm 17.7				
134.....								7.820	0.6 \pm 0.2
135.....	Fe XVIII	14.549	$2s^2 2p^5 2P_{3/2}-2s^2 2p^4 ({}^3P) 3d {}^4P_{3/2}$	14.555	107.0 \pm 13.6				
136.....								7.827	0.5 \pm 0.2
137.....						11.311	9.4 \pm 1.7		
138.....	Fe XVIII	14.584	$2s^2 2p^5 2P_{3/2}-2s^2 2p^4 ({}^3P) 3d {}^4P_{1/2}$	14.584	60.2 \pm 8.2				
139.....	Fe XVIII	11.324	$2s^2 2p^5 2P_{3/2}-2s^2 2p^4 ({}^1D) 4d {}^2F_{5/2}$			11.324	44.3 \pm 2.8		
	Fe XVIII	11.324	$2s^2 2p^5 2P_{3/2}-2s^2 2p^4 ({}^1D) 4d {}^2S_{1/2}$						
	Fe XVIII	11.354	$2s^2 2p^5 2P_{3/2}-2s^2 2p^4 ({}^1D) 4d {}^2P_{3/2}$						
140.....	Fe XVIII	14.610	$2s^2 2p^5 2P_{1/2}-2s^2 2p^4 ({}^3P) 3d {}^2P_{3/2}$	14.610	20.6 \pm 6.5				
143.....	Mg XI	7.850	$1s^2 {}^1S_0-1s 3p {}^1P_1$					7.850	17.2 \pm 0.5
146.....	Fe XIX	14.669	$2s^2 2p^4 {}^3P_2-2s^2 2p^3 ({}^2D) 3s {}^3D_3$	14.669	83.9 \pm 9.4				
	Fe XVIII	14.670	$2s^2 2p^5 2P_{1/2}-2s^2 2p^4 ({}^3P) 3d {}^2D_{3/2}$						
149.....	Al XII	7.872	$1s^2 {}^1S_0-1s 2s {}^3S_1$					7.872	5.5 \pm 0.3
	Al XI (d)	7.872	$1s^2 2p {}^2P_{1/2}-1s 2p^2 {}^2D_{3/2}$						
	Al XI (d)	7.876	$1s^2 2p {}^2P_{3/2}-1s 2p^2 {}^2D_{5/2}$						
149.....				14.703	15.0 \pm 4.6				
153.....	Fe XIX	14.738	$2s^2 2p^4 {}^3P_2-2s^2 2p^3 ({}^2D) 3s {}^3D_2$	14.741	25.8 \pm 6.4				
	Fe XIX	14.737	$2s^2 2p^4 {}^1D_2-2s^2 2p^3 ({}^2P) 3s {}^3P_2$						
154.....	Fe XX	14.764	$2s 2p^4 {}^4P_{5/2}-2s^2 2p^2 ({}^3P) 3p {}^4S_{3/2}$	14.756	19.0 \pm 6.4				
155.....	Fe XVIII	14.769	$2s^2 2p^5 2P_{1/2}-2s^2 2p^4 ({}^3P) 3d {}^4P_{3/2}$	14.767	14.3 \pm 6.4				
157.....	Fe XVIII	11.420	$2s^2 2p^5 2P_{3/2}-2s^2 2p^4 ({}^3P) 4d {}^2F_{5/2}$			11.420	36.5 \pm 2.4		
	Fe XVII	11.420	$2s^2 2p^6 {}^1S_0-2s^2 2p^5 5s {}^1P_1$						
160.....	O VIII	14.821	$1s {}^2S_{1/2}-5p {}^2P_{3/2}$	14.819	20.7 \pm 4.4				
	O VIII	14.821	$1s {}^2S_{1/2}-5p {}^2P_{1/2}$						
161.....						11.441	15.2 \pm 1.7		
164.....	Fe XVIII	11.456	$2s^2 2p^5 2P_{1/2}-2s^2 2p^4 ({}^1D) 4d {}^2D_{3/2}$			11.456	9.5 \pm 1.5		
	Fe XVIII	11.456	$2s^2 2p^5 2P_{3/2}-2s^2 2p^4 ({}^3P) 4d {}^4D_{3/2}$						
	Fe XVIII	11.457	$2s^2 2p^5 2P_{1/2}-2s^2 2p^4 ({}^1D) 4d {}^2S_{1/2}$						
169.....	Fe XVIII	11.469	$2s^2 2p^5 2P_{1/2}-2s^2 2p^4 ({}^1D) 4d {}^2P_{3/2}$			11.480	4.9 \pm 1.4		
169.....	Fe XX	14.913	$2s 2p^4 {}^4P_{3/2}-2s^2 2p^2 ({}^3P) 3p {}^4S_{3/2}$	14.910	25.4 \pm 5.0				
171.....	Fe XVIII	14.932	$2s^2 2p^5 2P_{1/2}-2s^2 2p^4 ({}^3P) 3d {}^4D_{3/2}$	14.932	24.9 \pm 5.2				
	Fe XIX	14.932	$2s^2 2p^4 {}^3P_1-2s^2 2p^3 ({}^2D) 3s {}^3D_1$						
	Fe XX	14.932	$2s 2p^4 {}^4P_{5/2}-2s^2 2p^2 ({}^3P) 3p {}^4P_{3/2}$						
	Fe XIX	14.935	$2s^2 2p^4 {}^3P_1-2s^2 2p^3 ({}^2D) 3s {}^3D_2$						
177.....	Fe XIX	14.992	$2s^2 2p^4 {}^3P_2-2s^2 2p^3 ({}^4S) 3s {}^3S_1$	14.992	138.5 \pm 25.4				
	Fe XIX	14.992	$2s^2 2p^4 {}^1D_2-2s^2 2p^3 ({}^2D) 3s {}^1D_2$						
177.....	Fe XVIII	11.525	$2s^2 2p^5 2P_{3/2}-2s^2 2p^4 ({}^3P) 4d {}^2D_{5/2}$			11.525	60.7 \pm 3.6		
	Fe XVIII	11.525	$2s^2 2p^5 2P_{3/2}-2s^2 2p^4 ({}^3P) 4d {}^2D_{3/2}$						
179.....	Ni XIX	11.539	$2p^6 {}^1S_0-2s 2p^6 3p {}^1P_1$			11.534	12.7 \pm 2.8		
179.....	Fe XVII	15.015	$2s^2 2p^6 {}^1S_0-2s^2 2p^5 3d {}^1P_1$	15.014	1554.5 \pm 75.2				
181.....	Ne IX	11.547	$1s^2 {}^1S_0-1s 3p {}^1P_1$			11.545	48.6 \pm 3.0		
181.....				15.039	209.7 \pm 25.7				
183.....								7.986	0.7 \pm 0.2
183.....	Fe XX	15.063	$2s 2p^4 {}^4P_{3/2}-2s^2 2p^2 ({}^3P) 3p {}^4D_{5/2}$	15.060	82.4 \pm 19.4				
	Fe XX	15.053	$2s 2p^4 {}^4P_{5/2}-2s^2 2p^2 ({}^3P) 3p {}^4D_{3/2}$						

TABLE 9—Continued

TIME	ION	λ_{pred}	TRANSITION	CHANNEL 1		CHANNEL 2		CHANNEL 3	
				λ_{obs}	Flux	λ_{obs}	Flux	λ_{obs}	Flux
185.....	Fe XIX	15.081	$2s^2 2p^4 3P_2-2s^2 2p^3 (4S) 3s 5S_2$	15.081	139.5 ± 20.4				
188.....				15.113	20.7 ± 12.3				
195.....	O VIII	15.176	$1s 2S_{1/2}-4p 2P_{3/2}$	15.180	98.7 ± 14.1				
	O VIII	15.177	$1s 2S_{1/2}-4p 2P_{1/2}$						
	Fe XIX	15.163	$2s^2 2p^4 3P_0-2s^2 2p^3 (4S) 3s 3S_1$						
	Fe XIX	15.180	$2s 2p^5 3P_1-2s 2p^4 (4P) 3s 3P_0$						
198.....	Fe XIX	15.208	$2s 2p^5 3P_2-2s 2p^4 (4P) 3s 3P_2$	15.208	169.4 ± 16.6				
200.....				15.236	82.1 ± 14.2				
203.....	Fe XVII	15.262	$2s^2 2p^6 1S_0-2s^2 2p^5 3d 3D_1$	15.263	736.7 ± 39.7				
205.....				15.289	102.8 ± 14.7				
Time Bin 3									
208.....	Mg x (d)	8.069	$1s^2 2p 2P_{1/2}-1s 2p (3P) 3p 2D_{3/2}$					8.070	1.8 ± 0.2
	Mg x (d)	8.069	$1s^2 2p 2P_{3/2}-1s 2p (3P) 3p 2D_{5/2}$						
214.....	Fe XVIII	15.372	$2s^2 2p^5 2P_{3/2}-2s^2 2p^4 (3P) 3p 2D_{5/2}$	15.372	38.1 ± 10.6				
	Fe XVIII	15.371	$2s^2 2p^5 2P_{3/2}-2s^2 2p^4 (3P) 3p 2D_{5/2}$						
	Fe XVIII	15.394	$2s^2 2p^5 2P_{3/2}-2s^2 2p^4 (3P) 3p 4D_{7/2}$						
217.....	Fe XIX	15.402	$2s 2p^5 1P_1-2s 2p^4 (2D) 3s 1D_2$	15.408	11.5 ± 7.6				
218.....	Fe XX	11.739	$2s^2 2p^3 4S_{3/2}-2s 2p^3 (3S) 3p 4P_{5/2}$			11.739	15.1 ± 1.7		
	Fe XXIII	11.736	$2s 2p 1P_1-2s 3d 1D_2$						
	Fe XVIII	11.730	$2s 2p^6 2S_{1/2}-2s^2 2p^4 (1D) 5p 2D_{3/2}$						
219.....	Fe XVIII	15.429	$2s 2p^6 2S_{1/2}-2s 2p^5 (1P) 3s 2P_{3/2}$	15.430	12.7 ± 7.9				
222.....	Fe XVII	15.450	$2s^2 2p^6 1S_0-2s^2 2p^5 3d 3P_1$	15.454	154.9 ± 12.1				
224.....	Fe XXII	11.769	$2s^2 2p 2P_{1/2}-2s^2 3d 2D_{3/2}$			11.770	25.3 ± 2.2		
225.....				15.491	58.4 ± 8.6				
227.....	Fe XX	15.515	$2s 2p^4 2D_{5/2}-2s^2 2p^2 (3P) 3p 4D_{7/2}$	15.515	38.5 ± 7.9				
	Fe XVIII	15.522	$2s^2 2p^5 2P_{1/2}-2s^2 2p^4 (1S) 3s 2S_{1/2}$						
228.....						11.790	4.5 ± 1.2		
234.....								8.156	0.9 ± 0.2
235.....	Ni XX	11.832	$2s^2 2p^5 2P_{3/2}-2p^4 (1D) 3d 2D_{5/2}$			11.826	9.9 ± 1.4		
	Ni XX	11.841	$2s^2 2p^5 2P_{3/2}-2p^4 (1D) 3d 2P_{3/2}$						
238.....	Fe XVIII	15.627	$2s^2 2p^5 2P_{3/2}-2s^2 2p^4 (1D) 3s 2D_{5/2}$	15.627	231.0 ± 14.3				
243.....				15.675	15.0 ± 5.8				
243.....	Ni XX	11.872	$2s^2 2p^5 2P_{3/2}-2p^4 (1D) 3d 2S_{1/2}$			11.865	3.4 ± 1.2		
	Ni XX	11.870	$2s^2 2p^5 2P_{3/2}-2p^4 (1D) 3d 2F_{5/2}$						
252.....	Fe XVIII	15.770	$2s^2 2p^5 2P_{3/2}-2s^2 2p^4 (3P) 3s 2P_{1/2}$	15.766	18.8 ± 5.9				
257.....	Fe XXII	11.936	$2s^2 2p 2P_{3/2}-2s^2 3d 2D_{3/2}$			11.934	3.7 ± 1.1		
	Fe XXI	11.938	$2s^2 2p^2 3P_0-2s 2p^2 (4P) 3p 3D_1$						
258.....	Fe XVIII	15.830	$2s^2 2p^5 2P_{3/2}-2s^2 2p^4 (3P) 3s 4P_{3/2}$	15.830	159.1 ± 11.4				
263.....	Fe XVIII	15.873	$2s^2 2p^5 2P_{1/2}-2s^2 2p^4 (1D) 3s 2D_{3/2}$	15.873	156.3 ± 11.3				
	Fe XVIII	15.873	$2s^2 2p^5 2P_{3/2}-2s^2 2p^4 (3P) 3s 4P_{1/2}$						
265.....	Fe XXI	11.975	$2s^2 2p^2 3P_0-2s 2p^2 (4P) 3p 5P_1$			11.974	6.2 ± 1.2		
267.....								8.260	0.9 ± 0.2
276.....	O VIII	16.006	$1s 2S_{1/2}-3p 2P_{3/2}$	16.007	480.1 ± 20.1				
	O VIII	16.007	$1s 2S_{1/2}-3p 2P_{1/2}$						
	Fe XVII	16.005	$2s^2 2p^6 1S_0-2s^2 2p^5 3p 1D_2$						
	Fe XVIII	16.007	$2s^2 2p^5 2P_{3/2}-2s^2 2p^4 (3P) 3s 2P_{3/2}$						
279.....	Fe XVIII	16.030	$2s^2 2p^5 2P_{1/2}-2s^2 2p^4 (3P) 3s 2P_{1/2}$	16.034	73.6 ± 9.2				
	Fe XIX	16.027	$2s 2p^5 3P_1-2s^2 2p^3 (2P) 3p 3P_0$						
283.....	Fe XVIII	16.076	$2s^2 2p^5 2P_{3/2}-2s^2 2p^4 (3P) 3s 4P_{5/2}$	16.076	458.6 ± 19.5				
286.....	Fe XIX	16.110	$2s 2p^5 3P_2-2s^2 2p^3 (2D) 3p 3P_2$	16.109	99.7 ± 8.9				
292.....	Fe XVIII	16.141	$2s 2p^6 2S_{1/2}-2s 2p^5 (3P) 3s 2P_{3/2}$	16.168	80.6 ± 8.0				
295.....	Fe XVII	12.123	$2s^2 2p^6 1S_0-2s^2 2p^5 4d 1P_1$			12.125	179.5 ± 25.3		
297.....	Ne X	12.132	$1s 2S_{1/2}-2p 2P_{3/2}$			12.134	223.6 ± 23.2		
	Ne X	12.138	$1s 2S_{1/2}-2p 2P_{1/2}$						
299.....	Fe XVII	16.239	$2s^2 2p^6 1S_0-2s^2 2p^5 3p 3P_2$	16.237	27.5 ± 6.1				
302.....						12.157	11.8 ± 1.5		
302.....	Fe XIX	16.272	$2s 2p^5 3P_1-2s^2 2p^3 (2D) 3p 3P_2$	16.273	29.7 ± 6.1				
	Fe XIX	16.273	$2s 2p^5 3P_2-2s^2 2p^3 (2D) 3p 1F_3$						
	Fe XVIII	16.274	$2s^2 2p^5 2P_{1/2}-2s^2 2p^4 (3P) 3s 2P_{3/2}$						
306.....	Fe XVIII	16.281	$2s 2p^6 2S_{1/2}-2s 2p^5 (3P) 3s 4P_{3/2}$	16.309	42.8 ± 6.6				

TABLE 9—Continued

TIME	ION	λ_{pred}	TRANSITION	CHANNEL 1		CHANNEL 2		CHANNEL 3	
				λ_{obs}	Flux	λ_{obs}	Flux	λ_{obs}	Flux
Time Bin 4									
309.....	Fe xvii	16.335	$2s^2 2p^6 1S_0-2s^2 2p^5 3p 3D_2$	16.340	46.4 ± 6.7				
	Fe xix	16.343	$2s 2p^5 3P_2-2s^2 2p^3 (2D) 3p 3D_3$						
311.....	Fe xxii	12.201	$2s 2p^2 2D_{3/2}-2s 2p (3P) 3d 2D_{5/2}$			12.199	3.1 ± 1.2		
	Fe xxi	12.204	$2s 2p^3 3D_1-2s 2p^2 (2P) 3d 3F_2$						
314.....	Mg xi (d)	8.406	$1s 3d 1D_2-2p 3d 1F_3$					8.408	1.0 ± 0.2
	Mg xi (d)	8.409	$1s 3p 1P_1-2s 3d 1D_2$						
317.....	Mg xii	8.419	$1s 2S_{1/2}-2p 2P_{3/2}$					8.420	26.9 ± 1.0
319.....	Mg xii	8.425	$1s 2S_{1/2}-2p 2P_{1/2}$					8.425	14.2 ± 0.9
321.....						12.252	6.9 ± 1.4		
324.....	Fe xvii	12.264	$2s^2 2p^6 1S_0-2s^2 2p^5 4d 3D_1$			12.263	104.4 ± 4.0		
326.....						12.275	9.3 ± 1.6		
328.....	Fe xxi	12.282	$2s^2 2p^2 3P_0-2s^2 2p 3d 3D_1$			12.285	45.7 ± 2.4		
338.....				16.622	31.1 ± 5.9				
352.....	Fe xxi	12.395	$2s^2 2p^2 3P_1-2s^2 2p 3d 3D_1$			12.398	14.0 ± 1.9		
353.....	Fe xvii	16.777	$2s^2 2p^6 1S_0-2s^2 2p^5 3s 3P_1$	16.778	1747.0 ± 100.0				
354.....						12.409	12.5 ± 1.8		
358.....	Ni xix	12.435	$2p^6 1S_0-2p^5 3d 1P_1$			12.429	44.6 ± 3.0		
	Fe xxi	12.422	$2s^2 2p^2 3P_1-2s^2 2p 3d 3D_2$						
361.....	Mg xi (d)	8.561	$1s 2p 1P_1-2p 2p 1D_2$					8.553	1.0 ± 0.3
361.....						12.443	6.7 ± 1.5		
365.....	Fe xxi	12.462	$2s^2 2p^2 3P_2-2s^2 2p 3d 3D_1$			12.460	8.8 ± 1.4		
	Fe xxi	12.462	$2s 2p^3 5S_2-2s 2p^2 (4P) 3d 5F_3$						
	Fe xix	12.471	$2s^2 2p^4 3P_2-2s 2p^4 (4P) 3d 3F_4$						
368.....	Fe xxi	8.573	$2s^2 2p^2 3P_0-2s^2 2p 5d 3D_1$					8.574	0.9 ± 0.3
374.....	Fe xxi	12.499	$2s^2 2p^2 3P_2-2s^2 2p 3d 3F_3$			12.501	7.6 ± 1.5		
	Fe xxi	12.500	$2s 2p^3 5S_2-2s 2p^2 (4P) 3d 5F_2$						
378.....	Fe xvii	12.526	$2s^2 2p^6 1S_0-2s^2 2p^5 4s 3P_1$			12.522	5.2 ± 1.5		
382.....	Fe xvii	17.050	$2s^2 2p^6 1S_0-2s^2 2p^5 3s 1P_1$	17.054	2350.0 ± 20.0				
384.....						12.550	4.5 ± 1.2		
386.....	Fe xvii	17.097	$2s^2 2p^6 1S_0-2s^2 2p^5 3s 3P_2$	17.099	2100.0 ± 4.0				
387.....	Fe xx	12.566	$2s^2 2p^3 4S_{3/2}-2s 2p^3 (5S) 3p 4P_{1/2}$			12.566	5.1 ± 1.2		
	Fe xxi	12.570	$2s^2 2p^2 3P_2-2s^2 2p 3d 3F_2$						
391.....	Fe xx	12.581	$2s^2 2p^3 4S_{3/2}-2s 2p^3 (3S) 3p 4P_{5/2}$			12.581	9.5 ± 1.4		
	Fe xx	12.581	$2s^2 2p^3 4S_{3/2}-2s 2p^3 (5S) 3p 4P_{3/2}$						
395.....	Fe xx	12.600	$2s 2p^4 4P_{3/2}-2s 2p^3 (3S) 3d 4D_{5/2}$			12.600	3.3 ± 1.1		
	Fe xx	12.600	$2s 2p^4 4P_{3/2}-2s 2p^3 (3S) 3d 4D_{3/2}$						
406.....	Ni xix	12.656	$2p^6 1S_0-2p^5 3d 3D_1$			12.652	14.8 ± 1.7		
412.....	Fe xvii	12.681	$2s^2 2p^6 1S_0-2s^2 2p^5 4s 1P_1$			12.681	7.3 ± 1.2		
418.....				17.397	52.8 ± 8.9				
428.....	Fe xxii	12.757	$2s 2p^2 2D_{3/2}-2s 2p (3P) 3s 2P_{1/2}$			12.752	4.5 ± 1.1		
428.....				17.501	59.2 ± 9.3				
431.....	Fe xviii	12.762	$2s^2 2p^5 2P_{3/2}-2s 2p^5 (3P) 3d 4D_{7/2}$			12.764	4.7 ± 1.1		
	Fe xviii	12.764	$2s^2 2p^5 2P_{3/2}-2s 2p^5 (3P) 3d 4D_{5/2}$						
433.....	Fe xxi	12.776	$2s^2 2p^2 1D_2-2s^2 2p 3d 3F_2$			12.774	2.7 ± 1.0		
	Fe xxi	12.776	$2s 2p^3 3D_1-2s 2p^2 (4P) 3d 3F_2$						
	Fe xxi	12.776	$2s 2p^3 3D_2-2s 2p^2 (4P) 3d 3F_2$						
441.....	Fe xx	12.812	$2s^2 2p^3 4S_{3/2}-2s^2 2p^2 (3P) 3d 4P_{1/2}$			12.812	22.5 ± 1.9		
	Fe xviii	12.816	$2s^2 2p^5 2P_{3/2}-2s 2p^5 (1P) 3p 2D_{5/2}$						
441.....	Fe xviii	17.591	$2s 2p^6 2S_{1/2}-2s^2 2p^4 (1D) 3p 2P_{3/2}$	17.624	$\pm 170.4 16.8$				
444.....	Fe xx	12.827	$2s^2 2p^3 4S_{3/2}-2s^2 2p^2 (3P) 3d 4P_{3/2}$			12.827	$\pm 34.1 2.2$		
447.....				17.679	$\pm 26.2 7.8$				
449.....	Fe xx	12.845	$2s^2 2p^3 4S_{3/2}-2s^2 2p^2 (3P) 3d 4P_{5/2}$			12.846	30.7 ± 2.0		
458.....	O vii	17.768	$1s^2 1S_0-1s 4p 1P_1$	17.782	26.8 ± 7.6				
462.....	Fe xx	12.906	$2s^2 2p^3 4S_{3/2}-2s^2 2p^2 (3P) 3d 2F_{5/2}$			12.904	8.0 ± 1.4		
466.....	Fe xix	12.924	$2s^2 2p^4 3P_2-2s 2p^4 (4P) 3p 3D_3$			12.924	10.5 ± 1.5		
	Fe xix	12.924	$2s^2 2p^4 3P_2-2s 2p^4 (4P) 3p 3D_2$						
	Fe xix	12.924	$2s^2 2p^4 3P_2-2s 2p^4 (4P) 3p 3S_1$						
472.....	Fe xx	12.951	$2s^2 2p^3 4S_{3/2}-2s^2 2p^2 (3P) 3d 4D_{5/2}$			12.951	10.7 ± 1.5		
476.....	Fe xx	12.966	$2s^2 2p^3 4S_{3/2}-2s^2 2p^2 (3P) 3d 2P_{3/2}$			12.966	5.4 ± 1.3		
	Fe xx	12.966	$2s 2p^4 4P_{5/2}-2s 2p^3 (3D) 3d 2G_{7/2}$						
	Fe xx	12.965	$2s^2 2p^3 2D_{3/2}-2s 2p^3 (5S) 3p 6P_{5/2}$						
479.....	Fe xx	12.982	$2s^2 2p^3 2D_{3/2}-2s^2 2p^2 (3P) 3d 2D_{5/2}$			12.982	4.6 ± 1.2		

TABLE 9—Continued

TIME	ION	λ_{pred}	TRANSITION	CHANNEL 1		CHANNEL 2		CHANNEL 3	
				λ_{obs}	Flux	λ_{obs}	Flux	λ_{obs}	Flux
Time Bin 5									
488.....	Fe XIX	13.018	$2s^2 2p^4 \ ^3P_2-2s 2p^4 \ (^4P) 3p \ ^3D_3$			13.018	7.4 ± 1.3		
495.....	Fe XX	13.052	$2s^2 2p^3 \ ^4S_{3/2}-2s^2 2p^2 \ (^3P) 3d \ ^4F_{5/2}$			13.052	10.3 ± 1.4		
	Fe XX	13.046	$2s^2 2p^3 \ ^2D_{5/2}-2s^2 2p^2 \ (^3P) 3d \ ^2D_{5/2}$						
	Fe XXI	13.049	$2s^2 2p^2 \ ^3P_0-2s^2 2p 3s \ ^3P_1$						
504.....	Fe XIX	13.091	$2s^2 2p^4 \ ^3P_2-2s 2p^4 \ (^4P) 3p \ ^5P_2$			13.091	6.0 ± 1.2		
	Fe XIX	13.091	$2s^2 2p^4 \ ^3P_2-2s 2p^4 \ (^4P) 3p \ ^5P_3$						
	Fe XX	13.091	$2s^2 2p^3 \ ^2D_{5/2}-2s^2 2p^2 \ (^3P) 3d \ ^2F_{7/2}$						
	Fe XX	13.091	$2s^2 2p^3 \ ^4S_{3/2}-2s^2 2p^2 \ (^3P) 3d \ ^4F_{3/2}$						
	Fe XX	13.091	$2s 2p^4 \ ^4P_{3/2}-2s 2p^3 \ (^3D) 3d \ ^4D_{5/2}$						
508.....	Fe XXII	8.976	$2s^2 2p \ ^2P_{1/2}-2s^2 4d \ ^2D_{3/2}$					8.976	1.1 ± 0.2
516.....	Fe XX	13.141	$2s^2 2p^3 \ ^2D_{3/2}-2s^2 2p^2 \ (^3P) 3d \ ^2F_{5/2}$			13.142	7.9 ± 1.3		
	Fe XVII	13.135	$2s^2 2p^6 \ ^1S_0-2s 2p^6 3d \ ^1D_2$						
	Fe XX	13.143	$2s^2 2p^3 \ ^2D_{5/2}-2s^2 2p^2 \ (^3P) 3d \ ^4P_{5/2}$						
520.....						13.161	10.2 ± 1.4		
543.....	Fe XIX	13.254	$2s^2 2p^4 \ ^3P_2-2s^2 2p^3 \ (^2P) 3d \ ^3D_3$			13.254	3.4 ± 1.1		
	Fe XX	13.254	$2s^2 2p^3 \ ^2P_{1/2}-2s^2 2p^2 \ (^3P) 3d \ ^4P_{1/2}$						
	Fe XXI	13.252	$2s^2 2p^2 \ ^3P_2-2s^2 2p 3s \ ^3P_1$						
	Ni XX	13.256	$2s^2 2p^5 \ ^2P_{3/2}-2p^4 \ (^3P) 3s \ ^2P_{3/2}$						
545.....	Fe XX	9.065	$2s^2 2p^3 \ ^4S_{3/2}-2s^2 2p^2 \ (^3P) 5d \ ^4P_{1/2}$					9.075	1.1 ± 0.2
	Fe XX	9.069	$2s^2 2p^3 \ ^4S_{3/2}-2s^2 2p^2 \ (^3P) 5d \ ^4P_{5/2}$						
	Fe XX	9.069	$2s^2 2p^3 \ ^4S_{3/2}-2s^2 2p^2 \ (^3P) 5d \ ^4P_{3/2}$						
546.....	Fe XX	13.267	$2s^2 2p^3 \ ^2D_{5/2}-2s^2 2p^2 \ (^3P) 3d \ ^4F_{7/2}$			13.268	3.1 ± 1.0		
	Fe XX	13.267	$2s^2 2p^3 \ ^2P_{1/2}-2s^2 2p^2 \ (^3P) 3d \ ^2P_{1/2}$						
	Fe XX	13.269	$2s^2 2p^3 \ ^2D_{5/2}-2s^2 2p^2 \ (^3P) 3d \ ^2P_{3/2}$						
550.....	O VII	18.627	$1s^2 \ ^1S_0-1s 3p \ ^1P_1$	18.628	67.3 ± 17.1				
551.....	Fe XX	13.293	$2s^2 2p^3 \ ^2D_{3/2}-2s^2 2p^2 \ (^3P) 3d \ ^4F_{5/2}$			13.289	2.4 ± 1.0		
556.....	Ni XX	13.309	$2s^2 2p^5 \ ^2P_{3/2}-2p^4 \ (^3P) 3s \ ^4P_{5/2}$			13.310	3.9 ± 1.1		
	Fe XIX	13.314	$2s 2p^5 \ ^3P_2-2s 2p^4 \ (^2P) 3d \ ^3D_3$						
559.....	Fe XVIII	13.326	$2s^2 2p^5 \ ^2P_{3/2}-2s 2p^5 \ (^3P) 3p \ ^4P_{5/2}$			13.322	5.2 ± 1.2		
	Fe XVIII	13.326	$2s^2 2p^5 \ ^2P_{3/2}-2s 2p^5 \ (^3P) 3p \ ^2P_{1/2}$						
572.....	Fe XVIII	13.378	$2s^2 2p^5 \ ^2P_{3/2}-2s 2p^5 \ (^3P) 3p \ ^2D_{5/2}$			13.376	4.2 ± 1.2		
	Fe XX	13.379	$2s^2 2p^3 \ ^2P_{3/2}-2s^2 2p^2 \ (^3P) 3d \ ^2P_{1/2}$						
578.....	Fe XX	13.405	$2s 2p^4 \ ^4P_{5/2}-2s 2p^3 \ (^5S) 3d \ ^4D_{7/2}$			13.402	5.8 ± 1.3		
	Fe XVIII	13.405	$2s^2 2p^5 \ ^2P_{3/2}-2s 2p^5 \ (^3P) 3p \ ^4D_{3/2}$						
581.....	Mg XI	9.169	$1s^2 \ ^1S_0-1s 2p \ ^1P_1$					9.169	34.2 ± 1.4
583.....								9.174	5.3 ± 1.1
585.....	Fe XIX	13.430	$2s^2 2p^4 \ ^3P_2-2s^2 2p^3 \ (^2D) 3d \ ^1F_3$			13.429	10.1 ± 2.0		
585.....	Mg X (d)	9.180	$1s^2 3d \ ^2D_{3/2}-1s 2p \ (^1P) 3d \ ^2F_{5/2}$					9.180	2.6 ± 0.4
	Mg X (d)	9.182	$1s^2 3d \ ^2D_{5/2}-1s 2p \ (^1P) 3d \ ^2F_{7/2}$						
588.....	Mg X (d)	9.189	$1s^2 3s \ ^2S_{1/2}-1s 2p \ (^1P) 3s \ ^2P_{1/2}$					9.189	1.0 ± 0.4
	Mg X (d)	9.190	$1s^2 3s \ ^2S_{1/2}-1s 2p \ (^1P) 3s \ ^2P_{3/2}$						
589.....	O VIII	18.967	$1s \ ^2S_{1/2}-2p \ ^2P_{3/2}$	18.972	1330.0 ± 4.0				
	O VIII	18.973	$1s \ ^2S_{1/2}-2p \ ^2P_{1/2}$						
589.....	Ne IX	13.447	$1s^2 \ ^1S_0-1s 2p \ ^1P_1$			13.447	103.6 ± 5.1		
	Fe XVIII	13.448	$2s^2 2p^5 \ ^2P_{3/2}-2s 2p^5 \ (^3P) 3p \ ^4D_{5/2}$						
590.....	Mg X (d)	9.193	$1s^2 3p \ ^2P_{3/2}-1s 2p \ (^1P) 3p \ ^2P_{3/2}$					9.193	1.9 ± 0.5
	Mg X (d)	9.194	$1s^2 3p \ ^2P_{1/2}-1s 2p \ (^1P) 3p \ ^2D_{3/2}$						
	Mg X (d)	9.195	$1s^2 3p \ ^2P_{3/2}-1s 2p \ (^1P) 3p \ ^2D_{5/2}$						
594.....	Fe XIX	13.462	$2s^2 2p^4 \ ^3P_0-2s^2 2p^3 \ (^2P) 3d \ ^3P_1$			13.466	31.5 ± 2.7		
	Fe XIX	13.456	$2s^2 2p^4 \ ^3P_2-2s^2 2p^3 \ (^2D) 3d \ ^3S_1$						
603.....	Fe XIX	13.506	$2s^2 2p^4 \ ^3P_2-2s^2 2p^3 \ (^2D) 3d \ ^3D_2$			13.505	34.9 ± 2.8		
	Fe XX	13.505	$2s 2p^4 \ ^4P_{3/2}-2s 2p^3 \ (^5S) 3d \ ^4D_{3/2}$						
	Fe XXI	13.507	$2s 2p^3 \ ^3D_1-2s 2p^2 \ (^4P) 3s \ ^3P_0$						
605.....	Mg XI	9.231	$1s^2 \ ^1S_0-1s 2p \ ^3P_1$					9.232	7.8 ± 0.5
	Mg XI	9.228	$1s^2 \ ^1S_0-1s 2p \ ^3P_2$						
607.....	Fe XIX	13.525	$2s^2 2p^4 \ ^3P_2-2s^2 2p^3 \ (^2D) 3d \ ^3D_3$			13.521	49.0 ± 3.3		
615.....	Ne IX	13.553	$1s^2 \ ^1S_0-1s 2p \ ^3P_1$			13.553	25.6 ± 2.4		
	Fe XIX	13.555	$2s^2 2p^4 \ ^3P_2-2s^2 2p^3 \ (^2D) 3d \ ^3P_2$						
	Fe XIX	13.550	$2s^2 2p^4 \ ^3P_2-2s^2 2p^3 \ (^2D) 3d \ ^1P_1$						

TABLE 9—Continued

TIME	ION	λ_{pred}	TRANSITION	CHANNEL 1		CHANNEL 2		CHANNEL 3	
				λ_{obs}	Flux	λ_{obs}	Flux	λ_{obs}	Flux
626.....	Mg x	9.284	$1s^2 2s^2 S_{1/2}-1s 2s (^3P) 2p^2 P_{1/2}$					9.285	1.0 ± 0.2
	Mg x	9.284	$1s^2 2s^2 S_{1/2}-1s 2s (^3P) 2p^2 P_{3/2}$						
	Mg x (d)	9.284	$1s^2 2s^2 S_0-1s 2s (^3P) 2p^2 P_{3/2}$						
	Mg x (d)	9.286	$1s^2 2s^2 S_0-1s 2s (^3P) 2p^2 P_{1/2}$						
636.....	Fe XIX	13.636	$2s^2 2p^4 ^3P_2-2s^2 2p^3 (^2D) 3d ^3G_3$			13.634	4.1 ± 1.3		
638.....	Mg XI	9.314	$1s^2 ^1S_0-1s 2s ^3S_1$					9.315	21.2 ± 0.9
639.....	Fe XIX	13.648	$2s^2 2p^4 ^3P_2-2s^2 2p^3 (^2D) 3d ^3F_3$			13.648	9.8 ± 1.4		
640.....	Mg x (d)	9.316	$1s^2 2p^2 P_{1/2}-1s 2p^2 ^2D_{3/2}$					9.320	2.7 ± 0.6
	Mg x (d)	9.320	$1s^2 2p^2 P_{3/2}-1s 2p^2 ^2D_{3/2}$						
	Mg x (d)	9.321	$1s^2 2p^2 P_{3/2}-1s 2p^2 ^2D_{5/2}$						
645.....	Fe XIX	13.672	$2s^2 2p^4 ^3P_1-2s^2 2p^3 (^2D) 3d ^3D_2$			13.671	8.1 ± 1.3		
	Fe XIX	13.672	$2s^2 2p^4 ^3P_1-2s^2 2p^3 (^2D) 3d ^3P_1$						
	Fe XIX	13.673	$2s^2 2p^4 ^3P_2-2s^2 2p^3 (^2D) 3d ^3F_2$						
Time Bin 6									
652.....	Ne IX	13.699	$1s^2 ^1S_0-1s 2s ^3S_1$			13.699	61.9 ± 3.7		
656.....						13.712	6.5 ± 1.7		
657.....								9.362	0.7 ± 0.2
659.....	Fe XIX	13.721	$2s^2 2p^4 ^3P_1-2s^2 2p^3 (^2D) 3d ^3P_2$			13.723	7.1 ± 1.6		
	Fe XIX	13.721	$2s^2 2p^4 ^1D_2-2s^2 2p^3 (^2P) 3d ^3F_3$						
662.....	Fe XIX	13.741	$2s^2 2p^4 ^1D_2-2s^2 2p^3 (^2D) 3d ^1F_3$			13.737	6.8 ± 1.3		
669.....								9.390	1.8 ± 0.3
673.....	Ni XIX	13.779	$2p^6 ^1S_0-2p^5 3s ^1P_1$			13.779	14.0 ± 1.6		
	Fe XX	13.781	$2s^2 2p^3 ^4S_{3/2}-2s^2 2p^2 (^3P) 3s ^4P_{5/2}$						
678.....	Fe XIX	13.799	$2s^2 2p^4 ^3P_2-2s^2 2p^3 (^4S) 3d ^3D_3$			13.796	19.2 ± 1.8		
686.....	Fe XVII	13.823	$2s^2 2p^6 ^1S_0-2s 2p^6 3p ^1P_1$			13.826	38.1 ± 2.6		
690.....	Fe XIX	13.841	$2s^2 2p^4 ^1D_2-2s^2 2p^3 (^2D) 3d ^3D_3$			13.842	7.1 ± 1.3		
	Fe XIX	13.843	$2s^2 2p^4 ^3P_1-2s^2 2p^3 (^2D) 3d ^3F_2$						
	Fe XIX	13.844	$2s^2 2p^4 ^3P_2-2s^2 2p^3 (^4S) 3d ^3D_2$						
	Fe XX	13.844	$2s^2 2p^3 ^4S_{3/2}-2s^2 2p^2 (^3P) 3s ^4P_{3/2}$						
703.....	Fe XVII	13.891	$2s^2 2p^6 ^1S_0-2s 2p^6 3p ^3P_1$			13.893	5.8 ± 1.1		
706.....	Fe XXI	9.475	$2s^2 2p^2 ^3P_0-2s^2 2p 4d ^3D_1$					9.476	0.7 ± 0.2
708.....	Ne X	9.481	$1s ^2S_{1/2}-5p ^2P_{3/2}$					9.482	0.8 ± 0.2
	Ne X	9.481	$1s ^2S_{1/2}-5p ^2P_{1/2}$						
715.....	Fe XIX	13.936	$2s^2 2p^4 ^3P_0-2s^2 2p^3 (^4S) 3d ^3D_1$			13.937	7.5 ± 1.2		
	Fe XIX	13.938	$2s^2 2p^4 ^3P_2-2s^2 2p^3 (^4S) 3d ^5D_2$						
	Fe XIX	13.938	$2s^2 2p^4 ^3P_2-2s^2 2p^3 (^4S) 3d ^5D_3$						
	Fe XIX	13.938	$2s 2p^5 ^3P_2-2s 2p^4 (^4P) 3d ^3D_3$						
	Fe XIX	13.938	$2s^2 2p^4 ^3P_2-2s^2 2p^3 (^4S) 3d ^5D_1$						
721.....	Fe XVIII	13.962	$2s^2 2p^5 ^2P_{3/2}-2s^2 2p^4 (^1S) 3d ^2D_{5/2}$			13.958	6.1 ± 1.1		
	Fe XIX	13.957	$2s^2 2p^4 ^1D_2-2s^2 2p^3 (^2D) 3d ^3G_3$						
	Fe XIX	13.962	$2s 2p^5 ^3P_2-2s 2p^4 (^4P) 3d ^3F_2$						
	Fe XIX	13.964	$2s^2 2p^4 ^3P_1-2s^2 2p^3 (^4S) 3d ^3D_1$						
735.....								9.543	1.1 ± 0.2
738.....	Fe XIX	14.017	$2s 2p^5 ^3P_1-2s 2p^4 (^4P) 3d ^3P_2$			14.021	1.9 ± 1.0		
	Fe XIX	14.017	$2s^2 2p^4 ^3P_1-2s^2 2p^3 (^4S) 3d ^3D_2$						
741.....						14.029	4.1 ± 1.1		
744.....	Ni XIX	14.043	$2p^6 ^1S_0-2p^5 3s ^3P_1$			14.043	17.3 ± 1.7		
	Fe XIX	14.042	$2s 2p^5 ^3P_2-2s 2p^4 (^4P) 3d ^3F_3$						
	Fe XIX	14.043	$2s 2p^5 ^3P_2-2s 2p^4 (^4P) 3d ^3D_2$						
754.....	Ni XIX	14.077	$2p^6 ^1S_0-2p^5 3s ^3P_2$			14.076	11.6 ± 1.4		
756.....						14.086	2.7 ± 1.0		
Time Bin 7									
777.....								9.635	1.5 ± 0.3
791.....	Fe XVIII	14.206	$2s^2 2p^5 ^2P_{3/2}-2s^2 2p^4 (^1D) 3d ^2D_{5/2}$			14.206	119.4 ± 5.7		
	Fe XVIII	14.209	$2s^2 2p^5 ^2P_{3/2}-2s^2 2p^4 (^1D) 3d ^2P_{3/2}$						
806.....	Fe XVIII	14.258	$2s^2 2p^5 ^2P_{3/2}-2s^2 2p^4 (^1D) 3d ^2S_{1/2}$			14.258	28.9 ± 3.5		
	Fe XVIII	14.259	$2s^2 2p^5 ^2P_{3/2}-2s^2 2p^4 (^1D) 3d ^2F_{5/2}$						
813.....	Ne X	9.708	$1s ^2S_{1/2}-4p ^2P_{3/2}$					9.712	2.4 ± 0.5
	Ne X	9.709	$1s ^2S_{1/2}-4p ^2P_{1/2}$						

TABLE 9—Continued

TIME	ION	λ_{pred}	TRANSITION	CHANNEL 1		CHANNEL 2		CHANNEL 3	
				λ_{obs}	Flux	λ_{obs}	Flux	λ_{obs}	Flux
837.....	Fe XVIII	14.363	$2s^2 2p^5 2P_{1/2}-2s^2 2p^4 ({}^1D) 3d 2D_{3/2}$			14.361	5.9 ± 2.5		
841.....	Fe XVIII	14.376	$2s^2 2p^5 2P_{3/2}-2s^2 2p^4 ({}^3P) 3d 2D_{5/2}$			14.375	21.6 ± 3.3		
852.....								9.792	1.6 ± 0.4
855.....	Fe XVIII	14.419	$2s^2 2p^5 2P_{1/2}-2s^2 2p^4 ({}^1D) 3d 2P_{3/2}$			14.421	7.6 ± 2.6		
	Fe XVIII	14.421	$2s^2 2p^5 2P_{3/2}-2s^2 2p^4 ({}^3P) 3d 4P_{5/2}$						
891.....	Fe XVIII	14.537	$2s^2 2p^5 2P_{3/2}-2s^2 2p^4 ({}^3P) 3d 2F_{5/2}$			14.536	21.2 ± 3.5		
897.....	Fe XVIII	14.549	$2s^2 2p^5 2P_{3/2}-2s^2 2p^4 ({}^3P) 3d 4P_{3/2}$			14.554	14.1 ± 3.5		
906.....	Fe XVIII	14.584	$2s^2 2p^5 2P_{3/2}-2s^2 2p^4 ({}^3P) 3d 4P_{1/2}$			14.583	5.4 ± 2.4		
915.....	Fe XVIII	14.610	$2s^2 2p^4 3P_1-2s^2 2p^3 ({}^4S) 3p 3P_2$			14.610	4.6 ± 2.2		
934.....	Fe XIX	14.669	$2s^2 2p^4 3P_2-2s^2 2p^3 ({}^2D) 3s 3D_3$			14.666	13.2 ± 3.3		
	Fe XVIII	14.670	$2s^2 2p^5 2P_{1/2}-2s^2 2p^4 ({}^3P) 3d 2D_{3/2}$						
1025.....	Fe XVIII	14.932	$2s^2 2p^5 2P_{1/2}-2s^2 2p^4 ({}^3P) 3d 4D_{3/2}$			14.925	6.4 ± 2.9		
	Fe XIX	14.932	$2s^2 2p^4 3P_1-2s^2 2p^3 ({}^2D) 3s 3D_1$						
	Fe XIX	14.935	$2s^2 2p^4 3P_1-2s^2 2p^3 ({}^2D) 3s 3D_2$						
	Fe XX	14.932	$2s 2p^4 4P_{5/2}-2s^2 2p^2 ({}^3P) 3p 4P_{3/2}$						

NOTES.—Time is in seconds from the start of the observations. Wavelengths are in Å. Fluxes are in 10^3 photons $\text{cm}^{-2} \text{s}^{-1}$.

and the FCS scans occur over the flare peak, blending lines from FeXXI–XXIV might be a problem.

The Ne x Ly δ /Ly γ (9.481/9.708) line ratio is an excellent temperature indicator for temperatures lower than $\simeq 2$ MK. However, the observed ratio of 0.67 is higher than the predicted ratio for all values of the electron temperature. This ratio did not give any problem in the August 25 spectrum, and since the fluxes in the July 2 spectrum are fairly strong, most likely the cause of the discrepancy is an unexplained line contributing to the 9.482 Å feature significantly in this flare but not in the cooler August 25 one.

The Mg xi x, y, and z lines are easily identifiable in the spectrum, and their ratio $(x = y)/y$ is an excellent tool to measure the electron density. Its measured value of 2.75 ± 0.17 is only slightly dependent on the electron temperature. Assuming $\log T$ (T in K) to be in the 6.9–7.1 range, as indicated by the BCS Ca xix line ratios (see next section), we derive a density in the $11.9 \leq \log N_e \leq 12.1$ range (N_e in cm^{-3}). If we assume the temperature value corresponding to the peak of Mg xi abundance, $\log T = 6.4$, the observed ratio is higher than the predicted one for any value of the electron density. The density value obtained assuming $6.9 \leq \log T \leq 7.1$ is lower than the value obtained from Fe line ratios, but it is also higher than typical active region values: this fact, together with the higher than predicted value of the observed ratio when $\log T = 6.4$, seems to indicate that both the flare plasma and the surrounding active region plasma contribute to the formation of the Mg xi lines.

6.5. Emission Measure from BCS Line and Continuum Emission

Line and continuum emission were used to measure the EM of the flare plasma, using the temperature obtained from the Ca xix line ratio. The results are shown in Figure 10, where we can see that the line EM is always slightly higher than the continuum EM, although the difference is within the uncertainties. The time dependence of the EM curves closely resemble that of the light curve of the band, but the emission measure peaks slightly after the light curve, and quite later than the temperature.

As for the August 25 data set, the consistency of the EM values measured from line or continuum emission cannot be used to draw conclusions about the Ca absolute abundance,

although the systematic shift between the two measurements might hint to some deviation of the Ca abundance from the adopted value from Feldman et al. (1992): in order to have agreement, the Ca absolute abundance should be increased by $\simeq 25\%$.

6.6. Emission Measure Analysis

We have applied the emission measure analysis also to the July 2 data set, by dividing the line list in five time bins and using all the isolated lines available in that wavelength range. The choice of the bin width was made as a compromise between having a time bin duration as short as possible, to minimize variations of the plasma conditions within it, and a sufficient number of ions to allow meaningful diagnostics.

However, the availability of only one FCS channel restricted the number of available ions and lines per ion to two or three at maximum (so the emission measure analysis gives only very uncertain results) prevents us from accurately measuring the temperature and the EM of the plasma, and even from determining whether the plasma is isothermal or not.

7. THE LINE LIST

The line list was compiled by comparing wavelengths and fluxes obtained from CHIANTI 5.0 with the measured values from both spectra. The temperatures and emission measure values determined from the emission measure analysis in § 5 and from the BCS line ratio diagnostics in § 6 have been used as input values in CHIANTI to calculate the predicted line fluxes for the August 25 and July 2 spectra, respectively. A nominal value of electron density, 10^{11}cm^{-3} , was chosen in the CHIANTI flux determination. This is not necessarily what is found from line ratios, but as most lines are not density-sensitive this choice is immaterial.

The line lists compiled from the 1980 August 25 and 1985 July 2 flare FCS spectra are given separately in Tables 9 and 10 (July 2), respectively. In the August 25 data set, 217 identifiable lines were observed, some at two times in FCS channels 1 and 2. We give transition identifications for 177 of them. For the July 2 spectrum recorded in FCS channel 3, some 83 identifiable lines were observed; we give transition identification for 60 of them.

TABLE 10
LINE LIST COMPILED FROM THE 1985 JULY 2 FCS SPECTRA

Time	Ion	λ_{pred}	Transition	λ_{obs}	Flux
1134.....	Fe xxiv	7.3700	$1s^2 2p^2 P_{1/2}-1s^2 5d^2 D_{3/2}$	7.368	1.2 ± 0.4
1164.....	Fe xxiv	7.4601	$1s^2 2p^2 P_{3/2}-1s^2 5s^2 S_{1/2}$	7.454	1.3 ± 0.4
1171.....	Mg xi	7.4731	$1s^2 {}^1S_0-1s 4p {}^1P_1$	7.473	20.4 ± 0.8
	Fe xxiii	7.4720	$2s^2 {}^1S_0-2s 5p {}^1P_1$		
1173.....				7.479	1.8 ± 0.6
1180.....				7.498	1.3 ± 0.5
1195.....				7.542	1.5 ± 0.5
15.....	Al xii	7.8721	$1s^2 {}^1S_0-1s 2s {}^3S_1$	7.871	2.8 ± 0.5
25.....				7.896	0.8 ± 0.3
27.....	Fe xxiii	7.8830	$2s 2p {}^1P_1-2s 5d {}^1D_2$	7.902	3.6 ± 0.5
33.....				7.919	2.2 ± 0.4
39.....	Fe xxiii	7.9437	$2s 2p {}^1P_1-2s 5s {}^1S_0$	7.934	1.5 ± 0.4
54.....				7.975	1.6 ± 0.5
59.....	Fe xxiv	7.9841	$1s^2 2s^2 S_{1/2}-1s^2 4p^2 P_{3/2}$	7.986	9.4 ± 0.5
62.....	Fe xxiv	7.9943	$1s^2 2s^2 S_{1/2}-1s^2 4p^2 P_{1/2}$	7.996	5.4 ± 0.4
71.....	Na xi	8.0209	$1s^2 S_{1/2}-4p^2 P_{3/2}$	8.019	1.0 ± 0.4
	Na xi	8.0214	$1s^2 S_{1/2}-4p^2 P_{1/2}$		
90.....	Mg xi (d)	8.0692	$1s^2 2p^2 P_{1/2}-1s 2p ({}^3P) 3p^2 D_{3/2}$	8.069	1.2 ± 0.3
	Mg xi (d)	8.0697	$1s^2 2p^2 P_{3/2}-1s 2p ({}^3P) 3p^2 D_{5/2}$		
98.....	Fe xxii	8.0910	$2s^2 2p^2 P_{1/2}-2s^2 5d^2 D_{3/2}$	8.090	4.0 ± 2.0
123.....				8.153	3.0 ± 0.5
126.....	Fe xxii	8.1650	$2s 2p^2 {}^4P_{3/2}-2s 2p ({}^3P) 5d^4 P_{5/2}$	8.161	1.7 ± 0.4
129.....	Fe xxii	8.1690	$2s^2 2p^2 P_{3/2}-2s^2 5d^2 D_{3/2}$	8.169	2.6 ± 0.4
	Fe xxii	8.1730	$2s^2 2p^2 P_{3/2}-2s^2 5d^2 D_{5/2}$		
154.....	Fe xxiv	8.2324	$1s^2 2p^2 P_{1/2}-1s^2 4d^2 D_{3/2}$	8.233	7.2 ± 0.7
176.....	Fe xxiv	8.2834	$1s^2 2p^2 P_{1/2}-1s^2 4s^2 S_{1/2}$	8.287	2.3 ± 0.5
183.....	Fe xxiii	8.3050	$2s^2 {}^1S_0-2s 4p {}^1P_1$	8.304	19.0 ± 0.7
185.....				8.310	4.7 ± 0.5
188.....	Fe xxiv	8.3164	$1s^2 2p^2 P_{3/2}-1s^2 4d^2 D_{5/2}$	8.317	19.1 ± 0.7
	Fe xxiii	8.3170	$2s^2 {}^1S_0-2s 4p {}^3P_1$		
231.....	Fe xxii	8.3310	$2s 2p^2 {}^2D_{3/2}-2s 2p ({}^3P) 5d^2 F_{5/2}$	8.323	3.6 ± 0.4
229.....	Mg xii	8.4192	$1s^2 S_{1/2}-2p^2 P_{3/2}$	8.419	167.3 ± 6.4
231.....	Mg xii	8.4246	$1s^2 S_{1/2}-2p^2 P_{1/2}$	8.424	105.5 ± 5.5
272.....	Mg xi (d)	8.5196	$1s 2s {}^3S_1-2s 2p {}^3P_1$	8.523	1.9 ± 0.5
	Mg xi (d)	8.5208	$1s 2s {}^3S_1-2s 2p {}^3P_2$		
276.....	Fe xxiii	8.5290	$2s 2p {}^3P_0-2s 4d^3 D_1$	8.532	2.7 ± 0.5
283.....	Fe xxiii	8.5500	$2s 2p {}^3P_1-2s 4d^3 D_2$	8.549	6.4 ± 0.5
	Fe xxiii	8.5516	$2s 2p {}^3P_1-2s 4d^3 D_1$		
293.....	Fe xxi	8.5730	$2s^2 2p^2 {}^3P_0-2s^2 2p 5d^3 D_1$	8.573	14.6 ± 0.8
311.....	Fe xxiii	8.6160	$2s 2p {}^3P_2-2s 4d^3 D_3$	8.615	8.9 ± 0.6
324.....	Fe xxi	8.6430	$2s^2 2p^2 {}^3P_2-2s^2 2p 5d^3 F_3$	8.644	4.3 ± 0.5
	Fe xxi	8.6470	$2s^2 2p^2 {}^3P_2-2s^2 2p 5d^3 F_2$		
	Fe xxi	8.6280	$2s^2 2p^2 {}^3P_1-2s^2 2p 5d^3 D_1$		
331.....				8.660	2.2 ± 0.5
334.....				8.667	1.1 ± 0.3
336.....				8.672	1.5 ± 0.5
340.....				8.678	2.3 ± 0.5
366.....	Fe xxii	8.7150	$2s^2 2p^2 P_{1/2}-2s 2p ({}^3P) 4p^2 D_{3/2}$	8.715	7.0 ± 0.6
369.....	Fe xxii	8.7220	$2s^2 2p^2 P_{1/2}-2s 2p ({}^3P) 4p^2 P_{1/2}$	8.722	4.0 ± 0.5
373.....				8.732	5.3 ± 0.5
376.....	Fe xxii	8.7410	$2s^2 2p^2 P_{1/2}-2s 2p ({}^3P) 4p^4 P_{3/2}$	8.738	4.5 ± 0.5
	Fe xxii	8.7350	$2s^2 2p^2 P_{3/2}-2s 2p ({}^3P) 4p^2 D_{5/2}$		
382.....	Fe xxii	8.7650	$2s^2 2p^2 P_{1/2}-2s 2p ({}^3P) 4p^4 D_{1/2}$	8.753	2.4 ± 0.4
410.....	Fe xxiii	8.8150	$2s 2p {}^1P_1-2s 4d {}^1D_2$	8.815	29.1 ± 0.9
421.....	Fe xxii	8.8320	$2s^2 2p^2 P_{3/2}-2s 2p ({}^3P) 4p^4 P_{3/2}$	8.840	1.2 ± 0.5
	Fe xxi	8.8230	$2s^2 2p^2 {}^3P_0-2s^2 2p^2 ({}^2S) 4p^3 P_1$		
425.....	Fe xxi	8.8550	$2s^2 2p^2 {}^1S_0-2s^2 2p 5d^3 D_1$	8.849	5.8 ± 0.8
451.....	Fe xxiii	8.9060	$2s 2p {}^1P_1-2s 4s {}^1S_0$	8.907	15.6 ± 0.8
457.....				8.919	5.5 ± 0.9
464.....	Fe xxiii	8.9287	$2p^2 {}^1S_0-2p 4d {}^1P_1$	8.935	1.7 ± 0.6
483.....	Fe xxii	8.9760	$2s^2 2p^2 P_{1/2}-2s^2 4d^2 D_{3/2}$	8.976	42.3 ± 1.2
491.....	Fe xxii	8.9930	$2s 2p^2 {}^4P_{1/2}-2s 2p ({}^3P) 4d^4 D_{1/2}$	8.993	3.0 ± 0.5
	Fe xxii	8.9950	$2s 2p^2 {}^4P_{1/2}-2s 2p ({}^3P) 4d^4 D_{3/2}$		
498.....	Fe xxii	9.0110	$2s 2p^2 {}^4P_{3/2}-2s 2p ({}^3P) 4d^2 F_{5/2}$	9.007	4.4 ± 0.5

TABLE 10—Continued

Time	Ion	λ_{pred}	Transition	λ_{obs}	Flux
505.....	Fe xxii	9.0270	$2s\ 2p^2\ 4P_{1/2}-2s\ 2p\ (^3P)\ 4d\ 4F_{3/2}$	9.023	3.4 ± 0.5
	Fe xxi	9.0250	$2s^2\ 2p^2\ 1S_0-2s\ 2p^2\ (^2P)\ 4p\ 3P_1$		
524.....	Fe xx	9.0650	$2s^2\ 2p^3\ 4S_{3/2}-2s^2\ 2p^2\ (^3P)\ 5d\ 4P_{1/2}$	9.062	4.0 ± 0.6
527.....	Fe xx	9.0689	$2s^2\ 2p^3\ 4S_{3/2}-2s^2\ 2p^2\ (^3P)\ 5d\ 4P_{5/2}$	9.069	11.8 ± 0.8
	Fe xx	9.0689	$2s^2\ 2p^3\ 4S_{3/2}-2s^2\ 2p^2\ (^3P)\ 5d\ 4P_{3/2}$		
	Fe xxii	9.0650	$2s\ 2p^2\ 4P_{3/2}-2s\ 2p\ (^3P)\ 4d\ 4F_{5/2}$		
530.....	Fe xxii	9.0730	$2s^2\ 2p\ 2P_{3/2}-2s^2\ 4d\ 2D_{3/2}$	9.075	16.7 ± 0.8
	Fe xxii	9.0730	$2s^2\ 2p\ 2P_{3/2}-2s^2\ 4d\ 2D_{5/2}$		
550.....	Fe xx	9.1100	$2s^2\ 2p^3\ 4S_{3/2}-2s^2\ 2p^2\ (^3P)\ 5d\ 2P_{3/2}$	9.115	5.1 ± 0.5
	Fe xx	9.1100	$2s^2\ 2p^3\ 4S_{3/2}-2s^2\ 2p^2\ (^3P)\ 5d\ 4F_{5/2}$		
560.....				9.137	6.1 ± 0.6
604.....	Mg xi	9.2282	$1s^2\ 1S_0-1s\ 2p\ 3P_2$	9.225	2.3 ± 0.7
608.....	Mg xi	9.2312	$1s^2\ 1S_0-1s\ 2p\ 3P_1$	9.233	32.3 ± 1.2
618.....	Fe xxii	9.2410	$2s\ 2p^2\ 2D_{3/2}-2s\ 2p\ (^3P)\ 4d\ 2F_{5/2}$	9.253	6.9 ± 1.0
638.....				9.292	10.1 ± 1.1
650.....	Mg xi	9.3144	$1s^2\ 1S_0-1s\ 2s\ 3S_1$	9.316	95.2 ± 2.5
667.....				9.348	4.7 ± 0.7
674.....	Fe xxii	9.3700	$2s\ 2p^2\ 2P_{1/2}-2s\ 2p\ (^3P)\ 4d\ 2D_{3/2}$	9.362	9.9 ± 0.9
686.....				9.384	10.9 ± 1.0
690.....	Fe xxii	9.3900	$2s\ 2p^2\ 2D_{3/2}-2s\ 2p\ (^3P)\ 4s\ 2P_{1/2}$	9.392	13.7 ± 0.9
703.....	Fe xxi	9.4120	$2s\ 2p^3\ 3D_1-2s\ 2p^2\ (^2P)\ 4d\ 3F_2$	9.417	1.8 ± 0.6
	Fe xxi	9.4100	$2s\ 2p^3\ 3D_2-2s\ 2p^2\ (^2S)\ 4d\ 3D_3$		
724.....				9.454	3.0 ± 0.6
736.....	Fe xxi	9.4750	$2s^2\ 2p^2\ 3P_0-2s^2\ 2p\ 4d\ 3D_1$	9.476	51.9 ± 3.6
738.....	Ne x	9.4807	$1s\ 2S_{1/2}-5p\ 2P_{3/2}$	9.481	11.1 ± 6.6
	Ne x	9.4809	$1s\ 2S_{1/2}-5p\ 2P_{1/2}$		
742.....				9.487	8.3 ± 4.2
762.....				9.523	0.8 ± 0.4
766.....				9.531	1.0 ± 0.4
775.....	Fe xxi	9.5420	$2s^2\ 2p^2\ 3P_1-2s^2\ 2p\ 4d\ 3D_1$	9.547	20.7 ± 1.5
	Fe xxi	9.5480	$2s^2\ 2p^2\ 3P_1-2s^2\ 2p\ 4d\ 3P_2$		
799.....	Fe xxi	9.5870	$2s^2\ 2p^2\ 3P_2-2s^2\ 2p\ 4d\ 3F_3$	9.587	4.1 ± 0.7
	Fe xxi	9.5820	$2s^2\ 2p^2\ 3P_2-2s^2\ 2p\ 4d\ 3D_1$		
825.....				9.633	2.2 ± 0.6
844.....				9.664	3.9 ± 0.8
860.....	Fe xix	9.6861	$2s^2\ 2p^4\ 3P_2-2s^2\ 2p^3\ (^2D)\ 5d\ 3S_1$	9.691	9.2 ± 1.0
	Fe xix	9.6939	$2s^2\ 2p^4\ 3P_2-2s^2\ 2p^3\ (^2D)\ 5d\ 3D_3$		
	Fe xxi	9.6900	$2s^2\ 2p^2\ 1S_0-2s^2\ 2p\ 4d\ 1P_1$		
	Fe xxi	9.6900	$2s\ 2p^3\ 3S_1-2s\ 2p^2\ (^2S)\ 4d\ 3D_2$		
873.....	Ne x	9.7080	$1s\ 2S_{1/2}-4p\ 2P_{3/2}$	9.713	16.7 ± 1.2
	Ne x	9.7085	$1s\ 2S_{1/2}-4p\ 2P_{1/2}$		
881.....	Fe xx	9.7207	$2s^2\ 2p^3\ 4S_{3/2}-2s\ 2p^3\ (^5S)\ 4p\ 4P_{5/2}$	9.726	5.4 ± 1.3
	Fe xx	9.7207	$2s^2\ 2p^3\ 4S_{3/2}-2s\ 2p^3\ (^5S)\ 4p\ 4P_{3/2}$		
	Fe xix	9.7207	$2s^2\ 2p^4\ 3P_2-2s^2\ 2p^3\ (^2D)\ 5d\ 3F_3$		
925.....				9.796	3.9 ± 0.7
932.....	Fe xxi	9.8140	$2s\ 2p^3\ 3D_1-2s\ 2p^2\ (^4P)\ 4d\ 3P_2$	9.806	5.6 ± 0.7
959.....	Fe xix	9.8458	$2s^2\ 2p^4\ 3P_2-2s^2\ 2p^3\ (^4S)\ 5d\ 3D_3$	9.848	7.4 ± 0.8
976.....	Fe xxi	9.9830	$2s\ 2p^3\ 3D_1-2s\ 2p^2\ (^4P)\ 4s\ 3P_0$	9.973	4.6 ± 0.7
	Ni xix	9.9771	$2p^6\ 1S_0-2p^5\ 4d\ 1P_1$		
1064.....	Fe xx	9.9965	$2s^2\ 2p^3\ 4S_{3/2}-2s^2\ 2p^2\ (^3P)\ 4d\ 4P_{1/2}$	9.998	8.1 ± 0.9
	Fe xx	9.9992	$2s^2\ 2p^3\ 4S_{3/2}-2s^2\ 2p^2\ (^3P)\ 4d\ 4P_{3/2}$		
	Fe xx	10.0042	$2s^2\ 2p^3\ 4S_{3/2}-2s^2\ 2p^2\ (^3P)\ 4d\ 4P_{5/2}$		

NOTES.—Wavelengths are in Å. Fluxes are in 10^3 photons cm^{-2} s^{-1} .

7.1. Line Identifications

Tables 9 and 10 show that most of the lines observed by FCS have been identified. The spectral lines belong to a number of ions, and within each ion they are emitted by many different configurations.

The ions contributing with at least one line to the observed spectra are listed in Table 11. They belong to the H-like and He-like isoelectronic sequences and to consecutive stages of ionization of Fe from Fe xvii to Fe xxiv. Also Ni xix, Ni xx, and Ni xxi emit lines identified in the observed spectra.

Nearly all the lines are emitted by levels excited by direct collisional excitation, but there are also a few lines emitted by levels beyond the ionization threshold of a few H-like and He-like ions, and excited by dielectronic recombination. For nearly all Fe ions, recombination to excited levels is a non-negligible excitation process, as shown by Gu (2003).

Interestingly, we find no evidence of the presence of L-shell dielectronic satellites to Fe xvii in the 15–17 Å range, previously reported by Phillips et al. (1982). No presence of observed transitions were found at the wavelengths where the strongest

TABLE 11

IONS PRESENT IN THE 1980 AUGUST 25 AND 1985 JULY 2 FCS SPECTRA

Element	Ionization Stage
O.....	VII, VIII
Ne.....	IX, X
Na.....	X, XI
Mg.....	X (d), XI, XI (d), XII
Al.....	XI (d), XII
Fe.....	XVII, XVIII, XIX, XX
	XXI, XXII, XXIII, XXIV
Ni.....	XIX, XX

NOTE.—The letter “d” indicates dielectronic lines.

Fe XVI(d) were predicted to fall by Cornille et al. (1994) and Phillips et al. (1997).

More detailed descriptions of the transitions in the spectrum, of their formation mechanisms, of their diagnostic use and of the comparison of their CHIANTI-predicted emissivities with the observations are beyond the scope of the present work and are postponed to a future paper (Landi et al. 2005b).

7.2. Energy Level Measurements

The large number of lines from Fe XVIII, Fe XIX, and Fe XX in the 1980 August 25 spectrum has allowed us to measure the energy of the upper levels that generate these lines. In many cases, energies from these levels have been observed in many occasions in the past, both from laboratory and astrophysical plasmas, but for many levels this is the first time that their energy is determined from observations. Additional energy levels for the $n = 4, 5$ configurations can be measured from the July 2

TABLE 12

Fe XVII ENERGY LEVEL MEASUREMENTS FROM THE FCS SPECTRA

Ion	Configuration	Level	E_{obs}	E_{pred}
Fe XVII.....	$2s^2 2p^5 3s$	3P_2	5848295	5839051.726
Fe XVII.....	$2s^2 2p^5 3s$	1P_1	5863727	5855229.911
Fe XVII.....	$2s^2 2p^5 3s$	3P_1	5960186	5951050.607
Fe XVII.....	$2s^2 2p^5 3p$	3D_2	6119951	6113104.193
Fe XVII.....	$2s^2 2p^5 3p$	3P_2	6158773	6150490.155
Fe XVII.....	$2s^2 2p^5 3p$	1D_2	6247267	6239469.187
Fe XVII.....	$2s^2 2p^5 3d$	3P_1	6470817	6461218.227
Fe XVII.....	$2s^2 2p^5 3d$	3D_1	6551792	6546467.771
Fe XVII.....	$2s^2 2p^5 3d$	1P_1	6660450	6660253.616
Fe XVII.....	$2s 2p^6 3p$	3P_1	7198128	7212598.037
Fe XVII.....	$2s 2p^6 3p$	1P_1	7232750	7247286.814
Fe XVII.....	$2s 2p^6 3d$	1D_2	7608902	7613165.150
Fe XVII.....	$2s^2 2p^5 4s$	1P_1	7885813	7864220.905
Fe XVII.....	$2s^2 2p^5 4s$	3P_1	7985945	7963743.522
Fe XVII.....	$2s^2 2p^5 4d$	3D_1	8154611	8130925.648
Fe XVII.....	$2s^2 2p^5 4d$	1P_1	8247423	8224314.004
Fe XVII.....	$2s^2 2p^5 5s$	1P_1	8756567	8749615.690
Fe XVII.....	$2s^2 2p^5 5s$	3P_1	8855827	8849780.236
Fe XVII.....	$2s^2 2p^5 5d$	3D_1	8888889	8886789.606
Fe XVII.....	$2s^2 2p^5 5d$	1P_1	8985533	8981638.547
Fe XVII.....	$2s 2p^6 4p$	3P_1	9057971	9055492.867
Fe XVII.....	$2s 2p^6 4p$	1P_1	9070295	9068092.200
Fe XVII.....	$2s^2 2p^5 6d$	1P_1	9285913	9275662.684
Fe XVII.....	$2s^2 2p^5 6d$	3D_1	9385265	9373203.394

NOTES.—Theoretical energy levels, listed for comparison purposes, have been taken from the calculations of E. Landi & M. F. Gu (2005, in preparation). Energies are in cm^{-1} .

TABLE 13

Fe XVIII ENERGY LEVEL MEASUREMENTS FROM THE FCS SPECTRA

Ion	Configuration	Level	E_{obs}	E_{pred}
Fe XVIII.....	$2s^2 2p^4 (^3P) 3s$	$^4P_{5/2}$	6220453	6212565.767
Fe XVIII.....	$2s^2 2p^4 (^3P) 3s$	$^2P_{3/2}$	6247267	6241056.287
Fe XVIII.....	$2s^2 2p^4 (^3P) 3s$	$^4P_{1/2}$	6300006	6290527.645
Fe XVIII.....	$2s^2 2p^4 (^3P) 3s$	$^4P_{3/2}$	6317119	6309561.528
Fe XVIII.....	$2s^2 2p^4 (^3P) 3s$	$^2P_{1/2}$	6340994	6335867.816
Fe XVIII.....	$2s^2 2p^4 (^1D) 3s$	$^2D_{5/2}$	6399181	6392733.663
Fe XVIII.....	$2s^2 2p^4 (^1D) 3s$	$^2D_{3/2}$	6402484	6396798.885
Fe XVIII.....	$2s^2 2p^4 (^3P) 3p$	$^2D_{5/2}$	6505334	6497176.094
Fe XVIII.....	$2s^2 2p^4 (^1S) 3s$	$^2S_{1/2}$	6547954	6544894.946
Fe XVIII.....	$2s^2 2p^4 (^1D) 3p$	$^2P_{3/2}$	6749292	6744800.188
Fe XVIII.....	$2s^2 2p^4 (^3P) 3d$	$^4D_{3/2}$	6799505	6802544.257
Fe XVIII.....	$2s^2 2p^4 (^3P) 3d$	$^4P_{1/2}$	6856829	6850357.627
Fe XVIII.....	$2s^2 2p^4 (^3P) 3d$	$^4P_{3/2}$	6873357	6865495.631
Fe XVIII.....	$2s^2 2p^4 (^3P) 3d$	$^2F_{5/2}$	6878998	6874691.361
Fe XVIII.....	$2s^2 2p^4 (^3P) 3d$	$^4F_{3/2}$	6903217	6895417.692
Fe XVIII.....	$2s^2 2p^4 (^3P) 3d$	$^2D_{3/2}$	6919277	6911329.063
Fe XVIII.....	$2s^2 2p^4 (^3P) 3d$	$^4P_{5/2}$	6934332	6927718.926
Fe XVIII.....	$2s^2 2p^4 (^3P) 3d$	$^2P_{3/2}$	6947105	6940494.002
Fe XVIII.....	$2s^2 2p^4 (^3P) 3d$	$^2D_{5/2}$	6956038	6952325.875
Fe XVIII.....	$2s^2 2p^4 (^1D) 3d$	$^2F_{5/2}$	7013115	7008947.553
Fe XVIII.....	$2s^2 2p^4 (^1D) 3d$	$^2S_{1/2}$	7013699	7010585.358
Fe XVIII.....	$2s^2 2p^4 (^1D) 3d$	$^2P_{3/2}$	7038045	7035426.630
Fe XVIII.....	$2s^2 2p^4 (^1D) 3d$	$^2D_{5/2}$	7039279	7041394.502
Fe XVIII.....	$2s^2 2p^4 (^1D) 3d$	$^2D_{3/2}$	7064720	7065970.929
Fe XVIII.....	$2s^2 2p^4 (^1D) 3d$	$^2P_{1/2}$	7076354	7072856.405
Fe XVIII.....	$2s^2 2p^4 (^1S) 3d$	$^2D_{5/2}$	7162298	7153536.142
Fe XVIII.....	$2s^2 2p^4 (^1S) 3d$	$^2D_{3/2}$	7182124	7176153.800
Fe XVIII.....	$2s 2p^5 (^3S) 3s$	$^4P_{3/2}$	7196286	7202607.771
Fe XVIII.....	$2s 2p^5 (^3P) 3s$	$^2P_{3/2}$	7260268	7257603.951
Fe XVIII.....	$2s 2p^5 (^3P) 3p$	$^4D_{5/2}$	7436050	7428666.203
Fe XVIII.....	$2s 2p^5 (^3P) 3p$	$^4D_{3/2}$	7459903	7454198.139
Fe XVIII.....	$2s 2p^5 (^3P) 3p$	$^2D_{5/2}$	7474959	7467574.777
Fe XVIII.....	$2s 2p^5 (^3P) 3p$	$^2P_{3/2}$	7487832	7494185.784
Fe XVIII.....	$2s 2p^5 (^3P) 3p$	$^2P_{1/2}$	7504127	7512644.195
Fe XVIII.....	$2s 2p^5 (^3P) 3p$	$^4P_{5/2}$	7504127	7513680.438
Fe XVIII.....	$2s 2p^5 (^1P) 3s$	$^2P_{3/2}$	7546028	7536063.772
Fe XVIII.....	$2s 2p^5 (^1P) 3p$	$^2D_{5/2}$	7805183	7802932.935
Fe XVIII.....	$2s 2p^5 (^3P) 3d$	$^4D_{5/2}$	7834535	7834750.754
Fe XVIII.....	$2s 2p^5 (^3P) 3d$	$^4D_{7/2}$	7834535	7835571.379
Fe XVIII.....	$2s 2p^5 (^3P) 3d$	$^2D_{3/2}$	7859011	7850005.428
Fe XVIII.....	$2s 2p^5 (^3P) 3d$	$^2P_{1/2}$	7876544	7876830.083
Fe XVIII.....	$2s 2p^5 (^3P) 3d$	$^2P_{3/2}$	7932040	7935061.506
Fe XVIII.....	$2s 2p^5 (^1P) 3d$	$^2P_{1/2}$	8139353	8138790.754
Fe XVIII.....	$2s 2p^5 (^1P) 3d$	$^2D_{3/2}$	8154857	8146250.225
Fe XVIII.....	$2s^2 2p^4 (^3P) 4d$	$^2D_{3/2}$	8676790	8658050.235
Fe XVIII.....	$2s^2 2p^4 (^3P) 4d$	$^2D_{5/2}$	8676790	8660810.924
Fe XVIII.....	$2s^2 2p^4 (^3P) 4d$	$^4D_{3/2}$	8729050	8725602.428
Fe XVIII.....	$2s^2 2p^4 (^3P) 4d$	$^2F_{5/2}$	8756567	8739356.642
Fe XVIII.....	$2s^2 2p^4 (^1D) 4d$	$^2S_{1/2}$	8830801	8811242.839
Fe XVIII.....	$2s^2 2p^4 (^1D) 4d$	$^2P_{3/2}$	8822040	8813069.186
Fe XVIII.....	$2s^2 2p^4 (^1D) 4d$	$^2F_{5/2}$	8830801	8816476.726
Fe XVIII.....	$2s^2 2p^4 (^1D) 4d$	$^2D_{3/2}$	8831528	8826785.987
Fe XVIII.....	$2s^2 2p^4 (^1S) 4d$	$^2D_{5/2}$	8949347	8958943.602
Fe XVIII.....	$2s^2 2p^4 (^3P) 5s$	$^4P_{1/2}$	9451796	9445790.594
Fe XVIII.....	$2s 2p^5 (^3P) 4p$	$^4P_{5/2}$	9451796	9453387.410
Fe XVIII.....	$2s 2p^5 (^3P) 4p$	$^2P_{3/2}$	9451796	9466379.579
Fe XVIII.....	$2s 2p^5 (^3P) 4p$	$^2D_{5/2}$	9451796	9469528.181
Fe XVIII.....	$2s^2 2p^4 (^3P) 5d$	$^2D_{3/2}$	9500192	9500772.990

NOTES.—Theoretical energy levels, listed for comparison purposes, have been taken from the calculations of E. Landi & M. F. Gu (2005, in preparation). Energies are in cm^{-1} .

TABLE 14—Continued

TABLE 14

Fe XIX ENERGY LEVEL MEASUREMENTS FROM THE FCS SPECTRA

Ion	Configuration	Level	E_{obs}	E_{pred}
Fe XIX	$2s^22p^3$ (4S) $3s$	5S_2	6630860	6620095.151
Fe XIX	$2s^22p^3$ (4S) $3s$	3S_1	6670224	6674289.905
Fe XIX	$2s^22p^3$ (2D) $3s$	3D_2	6785134	6776873.007
Fe XIX	$2s^22p^3$ (2D) $3s$	3D_1	6786468	6779444.168
Fe XIX	$2s^22p^3$ (2D) $3s$	3D_3	6817097	6810000.282
Fe XIX	$2s^22p^3$ (2D) $3s$	1D_2	6839076	6830941.245
Fe XIX	$2s^22p^3$ (2P) $3s$	3P_2	6952652	6956266.058
Fe XIX	$2s^22p^3$ (2D) $3p$	3D_3	7042841	7048247.979
Fe XIX	$2s^22p^3$ (2D) $3p$	1F_3	7068038	7068559.813
Fe XIX	$2s^22p^3$ (2D) $3p$	3P_2	7130244	7131404.362
Fe XIX	$2s^22p^3$ (4S) $3d$	5D_3	7174631	7167415.395
Fe XIX	$2s^22p^3$ (4S) $3d$	5D_2	7174631	7167891.919
Fe XIX	$2s^22p^3$ (4S) $3d$	5D_1	7174631	7168604.243
Fe XIX	$2s^22p^3$ (4S) $3d$	3D_2	7223491	7216760.237
Fe XIX	$2s^22p^3$ (4S) $3d$	3D_1	7250810	7243658.734
Fe XIX	$2s^22p^3$ (4S) $3d$	3D_3	7246902	7244141.657
Fe XIX	$2s^22p^3$ (2D) $3d$	3F_2	7313503	7309698.652
Fe XIX	$2s^22p^3$ (2D) $3d$	3F_3	7327081	7321397.610
Fe XIX	$2s^22p^3$ (2D) $3d$	3G_3	7333685	7328143.771
Fe XIX	$2s^22p^3$ (2D) $3d$	3D_1	7341636	7332982.852
Fe XIX	$2s^22p^3$ (2D) $3d$	3P_2	7377446	7373010.864
Fe XIX	$2s^22p^3$ (2D) $3d$	1P_1	7377896	7380178.414
Fe XIX	$2s^22p^3$ (2D) $3d$	3D_3	7393777	7394339.741
Fe XIX	$2s^22p^3$ (2D) $3d$	3D_2	7403889	7400676.820
Fe XIX	$2s^22p^3$ (2D) $3d$	3P_1	7403660	7402234.876
Fe XIX	$2s^22p^3$ (2D) $3d$	3S_1	7431778	7423220.144
Fe XIX	$2s^22p^3$ (2D) $3d$	1F_3	7446192	7446722.916
Fe XIX	$2s^22p^3$ (2P) $3d$	3F_3	7456951	7460847.322
Fe XIX	$2s^22p^3$ (2P) $3d$	3P_1	7503567	7496758.915
Fe XIX	$2s2p^4$ (4P) $3s$	3P_2	7498377	7501603.411
Fe XIX	$2s^22p^3$ (2P) $3d$	3D_3	7544892	7538386.826
Fe XIX	$2s2p^4$ (4P) $3s$	3P_0	7572355	7573578.710
Fe XIX	$2s2p^4$ (4P) $3p$	5P_3	7638836	7630051.721
Fe XIX	$2s2p^4$ (4P) $3p$	5P_2	7638836	7631238.600
Fe XIX	$2s2p^4$ (4P) $3p$	3D_3	7681672	7677133.567
Fe XIX	$2s2p^4$ (4P) $3p$	3S_1	7737543	7728709.408
Fe XIX	$2s2p^4$ (4P) $3p$	5D_3	7737543	7731723.618
Fe XIX	$2s2p^4$ (4P) $3p$	3D_2	7737543	7737168.200
Fe XIX	$2s2p^4$ (2D) $3s$	1D_2	7758999	7775755.809
Fe XIX	$2s2p^4$ (4P) $3d$	3F_4	8025682	8018606.295
Fe XIX	$2s2p^4$ (4P) $3d$	3F_3	8044363	8039110.609
Fe XIX	$2s2p^4$ (4P) $3d$	3F_2	8085188	8083920.597
Fe XIX	$2s2p^4$ (4P) $3d$	3D_3	8097521	8097792.465
Fe XIX	$2s2p^4$ (4P) $3d$	3P_2	8118934	8116960.739
Fe XIX	$2s2p^4$ (2P) $3d$	3D_3	8435474	8439916.476
Fe XIX	$2s^22p^3$ (4S) $4d$	3D_2	9236115	9225609.947
Fe XIX	$2s^22p^3$ (4S) $4d$	3D_1	9236061	9233341.647
Fe XIX	$2s^22p^3$ (4S) $4d$	3D_3	9245562	9236196.852
Fe XIX	$2s^22p^3$ (2D) $4d$	3F_2	9344416	9343693.369
Fe XIX	$2s^22p^3$ (2D) $4d$	3F_3	9359790	9350312.523
Fe XIX	$2s^22p^3$ (2D) $4d$	3D_2	9383121	9363579.383
Fe XIX	$2s^22p^3$ (2D) $4d$	3P_1	9383121	9368663.618
Fe XIX	$2s^22p^3$ (2D) $4d$	3D_3	9385265	9388071.139
Fe XIX	$2s^22p^3$ (2D) $4d$	3P_2	9397613	9395194.384
Fe XIX	$2s^22p^3$ (2D) $4d$	1D_2	9405021	9408833.405
Fe XIX	$2s^22p^3$ (2D) $4d$	3S_1	9405295	9405230.923
Fe XIX	$2s^22p^3$ (2D) $4d$	1F_3	9423827	9413552.370
Fe XIX	$2s^22p^3$ (2P) $4d$	3D_1	9480818	9481383.191

Ion	Configuration	Level	E_{obs}	E_{pred}
Fe XIX	$2s2p^4$ (4P) $4d$	5P_2	10029529	10035514.577
Fe XIX	$2s2p^4$ (4P) $4d$	5F_3	10029529	10035998.977
Fe XIX	$2s^22p^3$ (4S) $5d$	3D_3	10154346	10156631.408
Fe XIX	$2s^22p^3$ (2D) $5d$	3F_3	10281719	10284351.641
Fe XIX	$2s^22p^3$ (2D) $5d$	3D_3	10318853	10315829.789
Fe XIX	$2s^22p^3$ (2D) $5d$	3S_1	10318853	10324119.730

NOTES.—Theoretical energy levels, listed for comparison purposes, have been taken from the calculations of E. Landi & M. F. Gu (2005, in preparation). Energies are in cm^{-1} .

TABLE 15

Fe XX ENERGY LEVEL MEASUREMENTS FROM THE FCS SPECTRA

Ion	Configuration	Level	E_{obs}	E_{pred}
Fe XX	$2s^22p^2$ (3P) $3s$	$^4P_{1/2}$	7157001	7150575.097
Fe XX	$2s^22p^2$ (3P) $3s$	$^4P_{3/2}$	7223346	7216554.958
Fe XX	$2s^22p^2$ (3P) $3s$	$^4P_{5/2}$	7256583	7259089.643
Fe XX	$2s^22p^2$ (3P) $3p$	$^4D_{3/2}$	7392890	7398300.108
Fe XX	$2s^22p^2$ (3P) $3p$	$^4P_{3/2}$	7449811	7445945.119
Fe XX	$2s^22p^2$ (3P) $3p$	$^4D_{5/2}$	7459692	7455681.369
Fe XX	$2s^22p^2$ (3P) $3p$	$^4D_{7/2}$	7503706	7497837.493
Fe XX	$2s^22p^2$ (3P) $3p$	$^4S_{3/2}$	7526133	7523433.426
Fe XX	$2s^22p^2$ (3P) $3d$	$^4F_{3/2}$	7638836	7634119.896
Fe XX	$2s^22p^2$ (3P) $3d$	$^4F_{5/2}$	7661661	7657677.311
Fe XX	$2s^22p^2$ (3P) $3d$	$^4F_{7/2}$	7713597	7708542.304
Fe XX	$2s^22p^2$ (3P) $3d$	$^2P_{3/2}$	7712479	7708559.533
Fe XX	$2s^22p^2$ (3P) $3d$	$^4D_{5/2}$	7721411	7717296.462
Fe XX	$2s^22p^2$ (1D) $3p$	$^2P_{3/2}$	7739697	7734316.440
Fe XX	$2s^22p^2$ (3P) $3d$	$^2F_{5/2}$	7748658	7747477.953
Fe XX	$2s2p^3$ (5S) $3s$	$^4S_{3/2}$	7757266.877	7757266.877
Fe XX	$2s^22p^2$ (3P) $3d$	$^4P_{5/2}$	7784907	7782096.827
Fe XX	$2s^22p^2$ (3P) $3d$	$^4P_{3/2}$	7796055	7794370.765
Fe XX	$2s^22p^2$ (3P) $3d$	$^2P_{1/2}$	7797774	7796359.563
Fe XX	$2s^22p^2$ (3P) $3d$	$^4P_{1/2}$	7805183	7803892.875
Fe XX	$2s^22p^2$ (3P) $3d$	$^2F_{7/2}$	7814934	7816042.759
Fe XX	$2s^22p^2$ (3P) $3d$	$^2D_{5/2}$	7841562	7843276.004
Fe XX	$2s2p^3$ (5S) $3p$	$^6P_{5/2}$	7851068	7855364.353
Fe XX	$2s2p^3$ (5S) $3p$	$^4P_{3/2}$	7948494	7940333.791
Fe XX	$2s2p^3$ (5S) $3p$	$^4P_{5/2}$	7948494	7940636.049
Fe XX	$2s2p^3$ (5S) $3p$	$^4P_{1/2}$	7957982	7948294.399
Fe XX	$2s2p^3$ (5S) $3d$	$^4D_{5/2}$	8219035	8217285.275
Fe XX	$2s2p^3$ (5S) $3d$	$^4D_{3/2}$	8225383	8219984.921
Fe XX	$2s2p^3$ (5S) $3d$	$^4D_{7/2}$	8212687	8223743.947
Fe XX	$2s2p^3$ (3D) $3d$	$^4D_{5/2}$	8459554	8459570.135
Fe XX	$2s2p^3$ (3D) $3d$	$^2G_{7/2}$	8465263	8469438.316
Fe XX	$2s2p^3$ (3S) $3p$	$^4P_{5/2}$	8518613	8512508.598
Fe XX	$2s2p^3$ (3S) $3d$	$^4D_{5/2}$	8757226	8754078.672
Fe XX	$2s2p^3$ (3S) $3d$	$^4D_{3/2}$	8757226	8756473.106
Fe XX	$2s^22p^2$ (3P) $4d$	$^4P_{5/2}$	10002000	9995817.375
Fe XX	$2s^22p^2$ (3P) $4d$	$^4P_{3/2}$	10002000	10000801.186
Fe XX	$2s^22p^2$ (3P) $4d$	$^4P_{1/2}$	10002000	10003565.812
Fe XX	$2s2p^3$ (5S) $4p$	$^4P_{5/2}$	10281719	10287342.715
Fe XX	$2s2p^3$ (5S) $4p$	$^4P_{3/2}$	10281719	10287379.143
Fe XX	$2s^22p^2$ (3P) $5d$	$^2P_{3/2}$	10970927	10982282.003
Fe XX	$2s^22p^2$ (3P) $5d$	$^4F_{5/2}$	10970927	10985786.030
Fe XX	$2s^22p^2$ (3P) $5d$	$^4P_{5/2}$	11026574	11029329.882
Fe XX	$2s^22p^2$ (3P) $5d$	$^4P_{3/2}$	11026574	11032416.458
Fe XX	$2s^22p^2$ (3P) $5d$	$^4P_{1/2}$	11035092	11034074.446

NOTES.—Theoretical energy levels, listed for comparison purposes, have been taken from the calculations of E. Landi & M. F. Gu (2005, in preparation). Energies are in cm^{-1} .

TABLE 16
Fe XXI ENERGY LEVEL MEASUREMENTS FROM THE FCS SPECTRA

Ion	Configuration	Level	E_{obs}	E_{pred}
Fe XXI	$2s^2 2p 3s$	3P_1	7661883	7663398.059
Fe XXI	$2s^2 2p 3p$	3P_0	7909861	7909434.068
Fe XXI	$2s^2 2p 3d$	3F_2	8074160	8072911.811
Fe XXI	$2s^2 2p 3d$	3F_3	8116728	8111336.477
Fe XXI	$2s^2 2p 3d$	3D_2	8119551	8118025.534
Fe XXI	$2s^2 2p 3d$	3D_1	8140908	8135992.161
Fe XXI	$2s 2p^2 (^4P) 3s$	3P_0	8181076	8179292.828
Fe XXI	$2s 2p^2 (^4P) 3p$	5P_1	8351428	8342324.568
Fe XXI	$2s 2p^2 (^4P) 3p$	3D_1	8379420	8373689.493
Fe XXI	$2s 2p^2 (^4P) 3d$	5F_2	8486331	8479898.213
Fe XXI	$2s 2p^2 (^4P) 3d$	5F_3	8512673	8497311.028
Fe XXI	$2s 2p^2 (^4P) 3d$	3F_2	8605427	8607148.814
Fe XXI	$2s 2p^2 (^2P) 3d$	3F_2	8974078	8980290.694
Fe XXI	$2s^2 2p 4d$	3F_3	10548160	10543488.120
Fe XXI	$2s^2 2p 4d$	3P_2	10548346	10542323.393
Fe XXI	$2s^2 2p 4d$	3D_1	10550615	10548345.907
Fe XXI	$2s^2 2p 4d$	1P_1	10690597	10680721.109
Fe XXI	$2s 2p^2 (^4P) 4s$	3P_0	10803758	10796641.467
Fe XXI	$2s 2p^2 (^4P) 4d$	3P_2	10974523	10969264.236
Fe XXI	$2s 2p^2 (^2S) 4p$	3P_1	11312217	11333617.005
Fe XXI	$2s 2p^2 (^2P) 4d$	3F_2	11395778	11404032.280
Fe XXI	$2s 2p^2 (^2S) 4d$	3D_3	11396460	11407370.901
Fe XXI	$2s 2p^2 (^2S) 4d$	3D_2	11414532	11415135.091
Fe XXI	$2s^2 2p 5d$	3D_1	11660681	11693599.342
Fe XXI	$2s^2 2p 5d$	3F_2	11682052	11682052.497
Fe XXI	$2s^2 2p 5d$	3F_3	11686086	11691360.467

NOTES.—Theoretical energy levels, listed for comparison purposes, have been taken from the calculations of E. Landi & M. F. Gu (2005, in preparation). Energies are in cm^{-1} .

TABLE 17
Fe XXII ENERGY LEVEL MEASUREMENTS FROM THE FCS SPECTRA

Ion	Configuration	Level	E_{obs}	E_{pred}
Fe XXII	$2s^2 3d$	$^2D_{3/2}$	8496931	8489631.510
Fe XXII	$2s 2p (^3P) 3s$	$^2P_{1/2}$	8578333	8574382.870
Fe XXII	$2s 2p (^3P) 3d$	$^2D_{5/2}$	8933819	8930632.763
Fe XXII	$2s^2 4d$	$^2D_{5/2}$	11137547	11138700.005
Fe XXII	$2s^2 4d$	$^2D_{3/2}$	11139184	11134653.489
Fe XXII	$2s 2p (^3P) 4s$	$^2P_{1/2}$	11383785	11390002.391
Fe XXII	$2s 2p (^3P) 4p$	$^4D_{1/2}$	11424654	11408997.383
Fe XXII	$2s 2p (^3P) 4p$	$^4P_{3/2}$	11437374	11440650.782
Fe XXII	$2s 2p (^3P) 4p$	$^2D_{3/2}$	11474469	11470625.517
Fe XXII	$2s 2p (^3P) 4p$	$^2P_{1/2}$	11474469	11460996.582
Fe XXII	$2s 2p (^3P) 4d$	$^4F_{5/2}$	11486766	11490365.817
Fe XXII	$2s 2p (^3P) 4d$	$^4F_{3/2}$	11487337	11479420.534
Fe XXII	$2s 2p (^3P) 4d$	$^4D_{3/2}$	11524309	11518849.937
Fe XXII	$2s 2p (^3P) 4d$	$^4D_{1/2}$	11524309	11521830.181
Fe XXII	$2s 2p (^3P) 4d$	$^2D_{3/2}$	11535055	11533950.036
Fe XXII	$2s 2p (^3P) 4d$	$^2F_{5/2}$	11553200	11540354.557
Fe XXII	$2s 2p (^3P) 4p$	$^2D_{5/2}$	11562530	11566280.807
Fe XXII	$2s^2 5d$	$^2D_{5/2}$	12359664	12352760.937
Fe XXII	$2s^2 5d$	$^2D_{3/2}$	12360302	12350622.487
Fe XXII	$2s 2p (^3P) 5d$	$^4P_{5/2}$	12713592	12705075.570
Fe XXII	$2s 2p (^3P) 5d$	$^2F_{5/2}$	12751324	12744016.634

NOTES.—Theoretical energy levels, listed for comparison purposes, have been taken from the calculations of E. Landi & M. F. Gu (2005, in preparation). Energies are in cm^{-1} .

TABLE 18
Fe XXIII ENERGY LEVEL MEASUREMENTS FROM THE FCS SPECTRA

Ion	Configuration	Level	E_{obs}	E_{pred}
Fe XXIII	$2s 3p$	3P_1	9079354	9074358.884
Fe XXIII	$2s 3p$	1P_1	9106639	9106100.892
Fe XXIII	$2s 3d$	1D_2	9271024	9274452.667
Fe XXIII	$2s 4s$	1S_0	11979536	11980285.600
Fe XXIII	$2s 4p$	3P_1	12023566	12023987.966
Fe XXIII	$2s 4p$	1P_1	12042389	12041659.718
Fe XXIII	$2s 4d$	3D_1	12072579	12073448.985
Fe XXIII	$2s 4d$	3D_2	12076400	12075008.518
Fe XXIII	$2s 4d$	3D_3	12079429	12077973.994
Fe XXIII	$2s 4d$	1D_2	12096710	12097770.413
Fe XXIII	$2p 4d$	1P_1	12614504	12638218.472
Fe XXIII	$2s 5s$	1S_0	13356394	13349489.537
Fe XXIII	$2s 5p$	1P_1	13381507	13381268.958
Fe XXIII	$2s 5d$	1D_2	13407435	13406983.529

NOTES.—Theoretical energy levels, listed for comparison purposes, have been taken from the calculations of E. Landi & M. F. Gu (2005, in preparation). Energies are in cm^{-1} .

data set for Fe XX to Fe XXIV, a few of which are also reported here for the first time.

The measured energy levels are reported in Tables 12–19. Theoretical values from the calculations of Landi & Gu (2005) (Fe XVII to Fe XXIII) and Zhang et al. (1990) (Fe XXIV) are also listed for comparison purposes. It is important to note that in many cases it is very difficult to associate the our estimate of the level energy with values from past work. This is because earlier studies before about 1990, when computers had more limited resources, used atomic models with fewer configurations than at present; also *LS*-coupling labeling of energy levels are often very different from ones obtained from more recent calculations such as those adopted in the present work. More recent measurements have been reported by Brown et al. (2002) using the *jj*-coupling scheme, but their energies could be matched to the present measurements using wavelength and flux correspondence between their laboratory spectra and the present data.

8. CONCLUSIONS

In the present work we have completely reanalyzed the two flare observations carried out by the FCS instrument on board *SMM*, in order to develop a comprehensive spectral atlas for solar flares in the 7–19 Å. We have carried out line identifications basing our selection on both line wavelength and flux, comparing

TABLE 19
Fe XXIV ENERGY LEVEL MEASUREMENTS FROM THE FCS SPECTRA

Ion	Configuration	Level	E_{obs}	E_{pred}
Fe XXIV	$4s$	$^2S_{1/2}$	12459076	12467560.000
Fe XXIV	$4p$	$^2P_{1/2}$	12506253	12512727.000
Fe XXIV	$4p$	$^2P_{3/2}$	12521913	12528858.000
Fe XXIV	$4d$	$^2D_{3/2}$	12538224	12546601.000
Fe XXIV	$4d$	$^2D_{5/2}$	12544323	12552248.000
Fe XXIV	$5s$	$^2S_{1/2}$	13936373	13933051.000
Fe XXIV	$5d$	$^2D_{3/2}$	13964187	13973378.000

NOTES.—Theoretical energy levels, listed for comparison purposes, have been taken from Zhang et al. (1990). Energies are in cm^{-1} .

the observed values with predictions from the CHIANTI atomic database. In order to calculate CHIANTI-based fluxes, we have carried out a complete analysis of the physical properties of the emitting plasmas in both flares using several different diagnostic techniques, and also data from the BCS instrument on board *SMM*. The emission measure, temperature, and, when possible, electron density of the emitting plasmas have been measured. In the case of the 1985 July 2 flare, very high densities of the order of 10^{13} cm^{-3} have been measured.

As a result, we have measured a total of 277 spectral lines, 237 of which (corresponding to 86% of the total) have been identified. Emitting ions belong to the H-like and He-like isoelectronic sequences, to eight consecutive stages of ionization of Fe (Fe xvii to Fe xxiv) and to Ni xix and Ni xx. Line iden-

tifications have allowed the measurement of the energies of the levels for the Fe ions included in the data set.

A by-product of this work is a complete assessment of the accuracy of the CHIANTI database in the 7–19 Å wavelength range. However, this assessment is beyond the scope of the present paper and will be the subject of a future publication.

The work of E. L. was supported by the NNH04AA12I, W10,232, and NNG04ED07P NASA grants. K. J. H. P. acknowledges support from a National Research Council Senior Research Associateship award. We thank the anonymous referee whose comments and suggestions helped to improve the original manuscript.

REFERENCES

- Acton, L. W., et al. 1980, *Sol. Phys.*, 65, 53
 Bely-Dubau, F., Gabriel, A. H., & Volonté, S. 1979, *MNRAS*, 186, 405
 Brown, G. V., Beiersdorfer, P., Liedahl, D. A., Widmann, K., Kahn, S. M., & Clothiaux, E. J. 2002, *ApJS*, 140, 589
 Cornille, M., Dubau, J., Faucher, P., Bely-Dubau, F., & Blancard, C. 1994, *A&AS*, 105, 77
 Dere, K. P., & Cook, J. W. 1979, *ApJ*, 229, 772
 Dere, K. P., Landi, E., Mason, H. E., Monsignori Fossi, B. C., & Young, P. R. 1997, *A&AS*, 125, 149
 Dubau, J., Gabriel, A. H., Loulergue, M., Steenman-Clark, L., & Volonté, S. 1981, *MNRAS*, 195, 705
 Fawcett, B. C., Jordan, C., Lemen, J. R., & Phillips, K. J. H. 1987, *MNRAS*, 225, 1013
 Feldman, U., Mandelbaum, P., Seely, J. L., Doschek, G. A., & Gursky, H. 1992, *ApJS*, 81, 387
 Gabriel, A. H. 1972, *MNRAS*, 160, 99
 Gu, M. F. 2003, *ApJ*, 582, 1241
 Landi, E., Del Zanna, G., Young, P. R., Dere, K. P., Mason, H. E., & Landini, M. 2005a, *ApJ*, submitted
 Landi, E., Feldman, U., Innes, D. E., & Curdt, W. 2003, *ApJ*, 582, 506
 Landi, E., & Gu, M. F. 2005, *ApJ*, submitted
 Landi, E., & Landini, M. 1997, *A&A*, 327, 1230
 Landi, E., Phillips, K. J. H., & Gu, M. F. 2005b, *ApJ*, submitted
 Landini, M., & Monsignori Fossi, B. C. 1970, *A&A*, 6, 468
 McKenzie, D. L., & Landecker, P. B. 1982, *ApJ*, 254, 309
 McKenzie, D. L., Landecker, P. B., Broussard, R. M., Ruge, H. R., Young, R. M., Feldman, U., & Doschek, G. A. 1980, *ApJ*, 241, 409
 McKenzie, D. L., Landecker, P. B., Feldman, U., & Doschek, G. A. 1985, *ApJ*, 289, 849
 Mazzotta, P., Mazzitelli, G., Colafrancesco, S., & Vittorio, N. 1998, *A&AS*, 133, 403
 Mewe, R. 1972, *Sol. Phys.*, 22, 459
 Mewe, R., Kaastra, J. S., & Liedahl, D. A. 1995, *Legacy*, 6, 16
 Parkinson, J. H. 1975, *Sol. Phys.*, 42, 183
 Phillips, K. J. H., Bhatia, A. K., Mason, H. E., & Zarro, D. M. 1996, *ApJ*, 466, 549
 Phillips, K. J. H., Greer, C. J., Bhatia, A. K., Coffey, I. H., Barnsley, R., & Keenan, F. P. 1997, *A&A*, 324, 381
 Phillips, K. J. H., Mewe, R., Harra-Murnion, L. K., Beiersdorfer, P., Brown, G. V., & Liedahl, D. A. 1999, *A&AS*, 138, 381
 Phillips, K. J. H., et al. 1982, *ApJ*, 256, 774
 Pottasch, S. R. 1963, *ApJ*, 137, 945
 Smith, R. K., Brickhouse, N. S., Liedahl, D. A., & Raymond, J. C. 2001, *ApJ*, 556, L91
 Young, P. R., Del Zanna, G., Landi, E., Dere, K. P., Mason, H. E., & Landini, M. 2003, *ApJS*, 144, 135
 Zhang, H. L., Sampson, D. H., & Fontes, C. J. 1990, *At. Data Nucl. Data Tables*, 44, 31